The electronic structure of fullerenes and fullerene compounds from high-energy spectroscopy

Golden, M.S.; Knupfer, M.; Fink, J.; Armbruster, J.F.; Cummins, T.R.; Romberg, H.A.; Roth, M.; Sing, M.; Schmidt, M.

DOI
10.1088/0953-8984/7/43/004

Publication date
1995

Published in
Journal of Physics-Condensed Matter

J. Phys.: Condens. Matter 7 (1995) 8219–8247. Printed in the UK

REVIEW ARTICLE

The electronic structure of fullerenes and fullerene compounds from high-energy spectroscopy

Mark S Golden†, Martin Knupfer†, Jörg Fink†, Johannes F Armbruster‡, Tom R Cummins‡, Hans A Romberg‡, Matthias Roth‡, Michael Sing‡, Michael Schmidt‡ and Erik Sohmen‡

† Institut für Festkörperforschung (IFF), IFW Dresden eV, PO Box 270016, D-01171 Dresden, Germany

‡ Forschungszentrum Karlsruhe, INFP, PO Box 3640, D-76021 Karlsruhe, Germany

Received 28 July 1995

Abstract. The high-energy spectroscopic study of the electronic structure of fullerenes and their compounds in the solid state is reviewed. It is shown that photoemission and electron energy-loss spectroscopy in transmission provide powerful tools for the experimental study of the electronic structure of solid C_{60}, C_{70} and higher fullerenes, as well as the compounds formed by their intercalation with alkali and alkaline-earth metals. Topical issues in the field are addressed, such as the role played by electron correlation, disorder and electron–phonon coupling.

1. Introduction

The discovery in 1985 of a third allotrope of pure carbon, the fullerenes, has presented solid state science with a new class of materials exhibiting fascinating and and potentially useful properties [1]. In this review, we aim to present the current status of research into the fullerenes and fullerene compounds from the standpoint of their electronic structure in the solid state, and in particular the role played in its study by high-energy spectroscopy. In the following, we concentrate mainly on data recorded in our own laboratories using high-energy electron energy-loss spectroscopy (EELS) in transmission, and photoemission spectroscopy (PES). However, we acknowledge at the outset the efforts of many other groups worldwide also engaged in the study of the electronic structure of these new solids, and stress that in some cases our data are representative of results first reported by other workers [2].

After the discovery of C_{60} and other fullerenes in the the soot produced by the laser vaporization of graphite by Kroto, Smalley and coworkers [1], the development of a process in which bulk quantities of these new molecules could be prepared in the laboratory by Krätschmer, Huffman *et al* [3]. in 1989 opened up the field of solid state fullerene science. To date there have been a number of review articles about fullerenes and their compounds [4], including more specialist articles covering the solid state properties of fullerenes [5], structural studies [6], theoretical aspects [7, 8], photoemission and inverse photoemission [9] as well as fullerene science viewed from a chemical perspective [10]. As there is certainly not space here for more than the briefest mention of most these areas, we direct the reader to these articles for a more detailed treatment.

0953-8984/95/438219+29$19.50

Before going on to discuss the experimental methods, data and theoretical models developed to describe the electronic structure of fullerenes and their compounds in the solid state, it is helpful to place such work in a broader context. Information from high-energy spectroscopic studies of fullerene electronic structure is of use in two main areas. The first of these is the testing of theoretical predictions. There have been many calculations of the electronic structure and physical properties of C_{60} and its compounds. The experimental determination of these properties, and in particular the details of the electronic structure, present a rigorous and direct test of any aspiring theory. At the same time, comparison of the high-energy spectroscopic data with different theoretical models can often help in the extraction of the essential physics of the system in question, since the models themselves are by necessity forced to describe only its defining features. In addition, many of the interesting and potentially useful properties of the fullerenes and their compounds, such as high electrical conductivity, superconductivity, and ferromagnetism, as well as their optical properties, are intimately related to their electronic structure, thus making the systematic study of fullerene electronic structure of some importance. The discussion of this study given below tends naturally to focus on the spectroscopic results from the archetypal fullerene, C_{60}. This mainly reflects the fact that the overwhelming majority of fullerene research conducted to date has been carried out on these materials' most abundant representative.

2. EELS and PES as probes of the electronic structure of solids

In this section we briefly describe the two experimental techniques with which most of the data discussed here were recorded. The salient points of the experimental set-up and sample preparation procedure will be given later. As its name suggests, the technique of electron energy-loss spectroscopy exploits the interaction of an electron beam of selected energy with the sample in question (usually a solid). The resulting excitations of the system are manifest in the outgoing electron beam as energy losses, which are expressed in terms of their energy separation from the incoming, or primary beam. At energies above 30 keV, the primary electron beam can be transmitted through thin samples and thus the electron energy-loss experiment can be carried out in transmission. Operation in transmission gives the dual advantages of bulk sensitivity (in comparison with other electron spectroscopic techniques such as EELS in reflection or photoemission) and the ability to measure energy losses at a well defined angle with respect to the direct beam, thus allowing the study of excitations as a function of momentum transfer. In addition, the energy loss can be set to zero and thus an electron diffraction experiment can be conducted in transmission, which allows *in situ* structural characterization of the sample under investigation.

The quantity measured in EELS is the loss function, $\mathrm{Im}(-1/\varepsilon)$, which provides information on the excitations of the system and, after Kramers–Kronig analysis (KKA), yields the real and imaginary parts of the dielectric function, $\varepsilon_1(\omega)$ and $\varepsilon_2(\omega)$, respectively. For energy losses below ~40 eV, the loss function essentially describes the valence band excitations of the system, and at higher energies, the loss function describes transitions from core or shallow core levels into unoccupied states of appropriate atomic character. If the effect of the resultant core hole is negligible, this gives a measure of the transition-matrix-element-weighted site- and symmetry-specific unoccupied density of electronic states (DOS). These core excitations are governed by the dipole selection rule, thus, for example, excitations from the C 1s core level of a carbon atom will give a picture of the unoccupied C 2p-derived DOS at that site. A more detailed description of the operation and principles behind such experiments can be found in [11]. Information analogous to that obtainable from EELS in the low-energy region is provided by optical spectroscopy (although only with

zero momentum transfer), and in the high-energy region from x-ray absorption spectroscopy (XAS).

The technique of photoemission is widely used in the study of the electronic structure of solids (see for example [12]). It utilizes the photoelectric effect in which an electron is ejected from the occupied electronic levels of the sample on irradiation with monochromatic light. The photoelectron flux as a function of the final state (kinetic) energy is a measure of the energy distribution of the $(N-1)$ electron states (where N is the number of electrons in the ground state). This is also known as the electron removal spectrum. For non-correlated systems this quantity is equivalent to a matrix-element-weighted measure of the *occupied DOS. If the sample under investigation is single crystalline, then the collection* of photoelectrons within a limited angular range (with respect to the sample normal) also determines the value of the component of the wavevector in the initial state parallel to the crystal surface, $k_{\parallel}$. In this way, both the energy and wavevector of the initial state can be probed, allowing the mapping of the electronic bands as a function of $k_{\parallel}$. The kinetic energy of the photoelectrons usually varies from a few electron volts up to a few hundred, depending on the photon energy used. This results in the surface sensitivity of the technique, as the inelastic mean free path of a typical photoelectron in a solid is in the range of 5–30 Å. This means that ultrahigh vacuum (UHV) is necessary to maintain a surface free of adsorbates during the timescale of the measurement, and that the effect of the surface should be taken into account in the interpretation of the resulting spectra. A complementary technique is that of inverse photoemission (IPES), in which the insertion of an electron into the unoccupied levels of a material is accompanied by emission of a photon. The number of photons emitted at a given energy is determined, thus giving the energy distribution of the $(N+1)$-electron system (the electron addition spectrum). IPES provides analogous information to the core level excitations carried out in an EELS or XAS experiment; however, IPES has the advantage of having no core hole present in the final state (although it does have a low cross-section for electron capture and is, like photoemission, a surface probe).

3. Experimental details

Fullerene containing soot was produced using the Krätschmer–Huffman carbon arc method [3]. After extraction with toluene, the C_{60} and C_{70} were separated using chromatography on an alumina column with 10% toluene in hexane as eluant. The remaining higher fullerenes were purified and separated using state of the art liquid chromatography [13]. Due primarily to the small quantities involved, but also to their chemical similarity and low solubility, the separation of the higher fullerenes in quantities sufficient for spectroscopic study is an important and exacting task so far achieved by only a few laboratories worldwide [13, 14].

The EELS experiments were performed in transmission with a primary beam energy of 170 keV in a purpose-built UHV spectrometer described in detail elsewhere [11]. The samples are made by vacuum sublimation of the appropriate fullerene from a heated crucible onto a substrate (usually an alkali halide single crystal) held at elevated temperature (~470 K). After deposition of ~1000 Å of fullerene (as monitored by a quartz crystal thickness monitor), the films are floated off the substrates in distilled water, mounted on standard electron microscopy grids and transferred into the EELS spectrometer. Intercalation is carried out *in situ* in the preparation chamber of the spectrometer (base pressure 5×10^{-10} mbar) by evaporation either from a commercial SAES getter source (alkali metals) or from a resistively heated evaporation cell (Ca). During intercalation, the fullerene film is maintained at ~470 K to promote intercalant homogeneity and to improve the grain

size of the resultant fulleride film. An additional post-anneal at higher temperature (up to 620 K) may also be used for the same purpose. Alternatively, phase pure fulleride samples can be prepared using vacuum distillation, in which either the fullerene or the intercalant is preferentially evaporated from the sample held at elevated temperature, such that the stoichiometry of a nominal starting composition approaches that of the desired phase. This technique has been shown in the past to be highly effective in the preparation of phase pure C_{60} and C_{70} fulleride thin-film samples [15, 16]. After preparation, the films are transferred into the spectrometer analysis chamber (base pressure 2×10^{-10} mbar) for measurement. For the valence level excitations and elastic scattering (electron diffraction) data shown here the momentum resolution of the instrument was set to 0.04 $Å^{-1}$ with an energy resolution of 90–140 meV. The core level excitations were performed with a momentum and energy resolution of 0.2 $Å^{-1}$ and 90–140 meV, respectively. All EELS experiments were conducted at room temperature.

The photoemission experiments were carried out using a commercial 50 mm mean radius hemispherical electron analyser, together with a noble gas discharge lamp providing radiation at energies of 21.22 and 16.8 eV for operation with He and Ne, respectively. The electron analyser is mounted on a goniometer allowing its independent rotation with respect to the sample surface in both the polar and azimuthal angles and has a total angular resolution of 2°. Ordered samples may additionally be characterized using low-energy electron diffraction (LEED). Fullerene films of ~100 Å in thickness are prepared *in situ* in the preparation chamber (base pressure 1×10^{-10} mbar) by sublimation from a Knudsen cell onto a heated substrate. The samples fall into two main categories: those deposited onto freshly evaporated polycrystalline gold films, and those grown on the cleaved (001) surface of GeS single crystals. The latter form ordered single-crystalline films, whilst the former are polycrystalline in morphology. Intercalation is carried out in the preparation chamber in a similar manner to that described above for the samples prepared for EELS studies. The samples are transferred *in vacuo* into the analysis chamber (base pressure 5×10^{-11} mbar), where they are mounted on a cryostat with a temperature range at the sample surface of 10–440 K.

4. Theoretical predictions of fullerene and fulleride electronic structure

Before discussing the experimental high-energy spectroscopic data from solid fullerenes and their compounds it is instructive to briefly consider the question of their electronic structure from the theoretical viewpoint. Due to its wide application, we will first discuss calculations based upon the local density approximation (LDA) to density functional theory, in which all many-body effects are collected into the exchange–correlation energy, which is evaluated within a free-electron model. We then discuss the extent to which this picture requires re-evaluation to take into account the effects of rotational disorder, electron correlation and electron–phonon/vibron coupling, all of which have a role to play in the determination of the electronic structure of fullerenes in the solid state.

4.1. LDA calculations

The molecular framework of the C_{60} molecule is built mainly upon sp^2-like σ bonds between the carbon nuclei; the π bonds lying on radii directed out on a line from the molecule's hollow centre. Thus on condensation of C_{60} into a solid, one would expect the majority of the intermolecular orbital overlap to be between the π MOs. The left-hand panel of figure 1 shows a schematic diagram of the MO scheme of an isolated C_{60} molecule, calculated

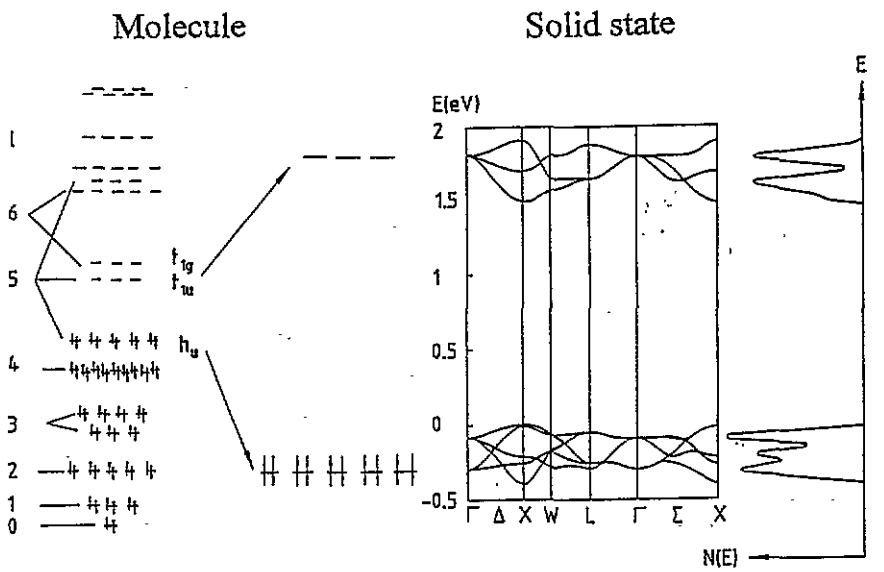

Figure 1. Left-hand panel, a schematic diagram of the C_{60} π MO energy scheme. The HOMO (h_u) and LUMO (t_{1u}) are shown in the expanded region. Centre panel. The bandstructure of the HOMO- and LUMO-derived bands of C_{60} in the solid state. Right-hand panel, the density of states of the HOMO- and LUMO-derived bands of solid C_{60} predicted from LDA calculations. (After Saito and Oshiyama [17].)

within a tight-binding representation. The icosahedral symmetry allows a maximum orbital degeneracy of five. Due to the quasispherical structure of the molecule, the electronic level scheme can be expanded in terms of spherical harmonics in the angular momentum, l [17, 18]. The highest occupied molecular orbital (HOMO) is fivefold degenerate (with h_{1u} symmetry and $l = 5$), and the lowest unoccupied molecular orbital (LUMO) is of t_{1u} symmetry (threefold degenerate, with $l = 5$). The next lowest unoccupied state, the LUMO + 1, has t_{1g} symmetry and is also triply degenerate. The large energy gap between the occupied and unoccupied π levels is in part responsible for the remarkable thermal stability of C_{60}.

The centre panel of figure 1 concentrates only on the bands derived from the molecular HOMO and LUMO, and shows that condensation into the solid (fcc with lattice constant $a_0 = 14.198$ Å) [19] has only a small effect on the electronic levels, calculated using the LDA [17]. A direct bandgap of the order of ~1.5 eV is predicted to remain between the HOMO- and LUMO-derived bands, the precise value of which differs slightly from one calculation to the next [7, 8, 17, 18]. Enough molecular character is retained such that the transition across the bandgap is essentially optically forbidden, as both HOMO- and LUMO-derived bands result from molecular levels possessing *ungerade* symmetry. The relatively weak van der Waals interactions between the C_{60} molecules in the solid are also expressed in a cohesive energy of only 1.6 eV/C_{60} cluster (compared for example with a typical C–C bond energy of ~3 eV) [17]. The right-hand panel of figure 1 illustrates the density of states (DOS) of the two bands straddling the bandgap, which are predicted to have a dispersive width of ~0.4 and ~0.5 eV, respectively [17].

C_{60} adopts an fcc structure at room temperature, and so there are two tetrahedral sites and one octahedral site available for intercalation per C_{60} molecule [6] The crystal structures of the known alkali metal C_{60} fulleride phases vary from rock-salt or orthorhombic for AC_{60},

fcc for A_3C_{60}, bct for A_4C_{60} and bcc for A_6C_{60} (with the exception of sodium: Na_6C_{60} remains fcc) [6, 21–23]. The formation of many of these structures can be understood in terms of the progressive occupation of the interstitial sites by the intercalant (further details can be found in [6] and [23]). The most intensively studied fullerides have been those of the alkali metals K and Rb with C_{60}, as metallic conductivity and superconductivity was first reported in the A_3C_{60} materials (A = K, Rb). In the A_xC_{60} systems, the alkali metal atom donates its outermost s electron to the fullerene host upon intercalation, thus forming a salt, such as NaCl.

As regards the electronic structure, the simplest possible approach with which to treat the effects of alkali metal intercalation is to take the calculated electronic structure of the solid fullerene, for example C_{60}, and move the Fermi level appropriately to account for the transfer of one electron per alkali metal atom intercalated. This approach is valid in the sense that the highest-energy scale in these systems is that of the fullerene molecule itself, and that on this scale the system remains relatively unaffected by the addition of up to six electrons [24]. The results of LDA bandstructure calculations of RbC_{60} [20], $(Rb, K)_3C_{60}$ [25, 26], $(Rb, K)_4C_{60}$ [8] and $(Cs, Rb, K, Na)_6C_{60}$ [26–28] (see also [7] and [8]) would appear to confirm the simple picture outlined above, with complete charge transfer to the fullerene molecule and an insulating ground state only predicted in the case of the A_6C_{60} fullerides, in which the t_{1u}-derived band is full. However, as will be discussed below, many of the high-energy spectroscopic data from the A_xC_{60} materials fall outside the rigid-band doping scheme and the LDA description, with the insulating nature of A_4C_{60} (A = K, Rb, Cs) being the notable example. Thus the description of fulleride electronic structure needs to be further refined beyond the already sophisticated LDA calculations.

4.2. Orientational disorder

It is well known that the fullerenes are apt to display orientational disorder in the solid state. At 300 K the C_{60} molecules rotate very rapidly (they are in fact more labile than in solution), resulting in a lattice with fcc symmetry and a lattice constant of $a_0 = 14.2$ Å [19]. Below ~260 K there is a first-order phase transition from fcc to an orientationally ordered simple cubic (sc) phase (the icosohedral point group symmetry of the C_{60} molecule is incompatible with a rotationally ordered fcc phase). The C_{60} molecules, however, continue to 'ratchet' from one preferred orientation to another. This rotation is finally frozen out on crossing a glass transition at ~90 K, which leaves ~85% of the C_{60} molecules in one orientation and the remaining 15% in another orientation of slightly higher energy [29]. In the A_3C_{60} materials (A = K, Rb), the C_{60} molecules display a binary (merohedral) orientational disorder, with statistical occupancy of the two molecular orientations which remains disordered even at low temperature [6, 30]. This disorder has been predicted to have significant effects on the bandstructure for these materials [20], with a smearing out of the fine structure in the t_{1u}-derived conduction band DOS, whose width remains unaffected by the disorder [31]. However, the results of a cluster Bethe lattice model of K_3C_{60} suggest that despite the disorder, the electronic states near E_F are best described using an effective Bloch wave vector, with a mean free path of ~20 Å, and that the states localized due to disorder lie only at the bottom or top of the band [32].

4.3. Quasiparticle bandstructure

LDA approaches calculate a system's ground state electronic structure, but the experiments to which they are often compared (PES and IPES) are excitation spectra. There has

been, however, a calculation of the electronic excitations of solid C_{60} [33] within the GW approximation. This method uses the basic LDA eigenvalues to obtain the electron excitation energies of the system. The latter include a treatment of the electron self-energy (in terms of a dynamically screened Coulomb interaction) and are thus more directly comparable with the results from high-energy spectroscopies than are the bare LDA eigenvalues. Using this method, the quasiparticle gap is predicted to be 2.15 eV with bandwidths of 0.9, 0.7 and 0.8 eV for the HOMO-, LUMO- and (LUMO+1)-derived bands, respectively [33]. These figures are much closer to the experimental value of ~2.3 eV for the PES/IPES gap [9, 34] and the HOMO bandwidth of ~1 eV [35]. (although it has been pointed out that the fact that the self-energy corrections themselves are of the same order of magnitude as the uncorrected bandwidths shows that solid C_{60} cannot be treated as an 'ordinary' semiconductor such as Si [36]).

4.4. Electron correlation

As a result of solid C_{60}'s molecular nature, the charge distribution is inhomogenous, with charge concentrated on the molecules themselves. This localization of charge is analogous to that in some materials with partially filled 3d and 4f levels, for which LDA is unable to correctly predict their electronic structure as its mean-field treatment of the exchange and correlation energies cannot account for the strong on-site Coulomb repulsion (U) resulting from the the spatial localization of the orbitals in question. U between two holes on the same C_{60} molecule has been determined from the comparison of the C KVV Auger spectrum of C_{60} (an $(N-2)$ final state in which the two holes are on the same molecule) with the self-convolution of the valence level PES (i.e. $(N-1)\otimes(N-1)$, in which the two holes are on different C_{60} molecules). The average value of U across the different bands was found to be 1.4–1.6 eV [34, 37]. Thus U is large in comparison to the bandwidth (~0.5–0.6 eV from conventional LDA bandstructure calculations [20]), and therefore raises the question as to whether solid fullerenes are not more appropriately described within models in which the strong correlation is more explicitly treated [38, 39]. As a result of this, it has been suggested that integer x A_xC_{60} phases should be Mott–Hubbard insulators, and accordingly that the superconductor 'K_3C_{60}' is non-stoichiometric and therefore a doped Mott–Hubbard insulator [34].

There has also been lively debate as to whether the intersite hopping energy, $V = 0.7$ eV, (which has been derived from a comparative autoionization study of condensed C_{60} and C_{60} matrix isolated in Xe) [40] should reduce U to a value of $U_{eff} = U - V$ which would then be comparable in size to the bandwidth [41]. The counter-argument is that the nearest-neighbour interaction is excitonic in character (and hence charge neutral), and that the full, unscreened U should determine the proposed transport gap of stoichiometric K_3C_{60} [39, 42]. It has also been proposed that the critical (i.e. minimum) value of the correlation energy, U_{crit}, required for the formation of a Mott insulator depends on both the degeneracy and filling (N) of the electronic system in question [38]. In [38], for the case of A_xC_{60}, the degeneracy of the t_{1u}-derived conduction states is taken to be three, with a maximum U_{crit} resulting for half filling, and a smaller U_{crit} resulting for four electrons in the t_{1u} levels (i.e. A_4C_{60}). This means that the U required to drive A_3C_{60} non-metallic is greater than the corresponding value for A_4C_{60}, which would be consistent with the metallic and non-metallic nature of the A_3C_{60} and A_4C_{60} fullerides respectively.

4.5. Jahn–Teller distortion

Further to the possibility that A_3C_{60} could be less 'U sensitive' (i.e. have a higher U_{crit}) than other fullerides just mentioned above, the inclusion of the possibility of a lifting of the t_{1u} threefold degeneracy [43] in a $(C_{60})^{n-}$ system as a result of Jahn–Teller (JT) distortion has also been considered [44, 45]. This has consequences for the magnitude of U itself. The phonon contribution to U in $(C_{60})^{n-}$ is found to be negative for odd n and positive for even n, which would also favour less correlated behaviour in A_3C_{60} as opposed to A_4C_{60}.

While it is generally accepted that JT coupling is important for the $(C_{60})^{n-}$ molecule, for example for an accurate description of the gas phase PES of $(C_{60})^-$ [46], the question as to whether such JT effects survive in the solid remains open. Such electron–phonon coupling processes in the A_3C_{60} fullerides are also of additional interest in the context of whether a phonon-mediated mechanism is responsible for the superconductivity and will certainly be the subject of further theoretical work in the future.

5. High-energy spectroscopic results from pristine fullerenes

The now familiar photoemission profile of a thin film of solid C_{60} is shown in figure 2 together with the C 1s excitation spectrum of C_{60} [35, 47]. As was discussed in section 2, these measurements provide a picture of the occupied and unoccupied DOS of solid C_{60}, respectively. What is striking is the sharp and well separated features in the low-energy region of the spectrum of the solid. This points to the high degeneracy of the electronic levels as expected from the high symmetry of the molecule and in general to the weak interaction between the fullerene molecules in the solid state.

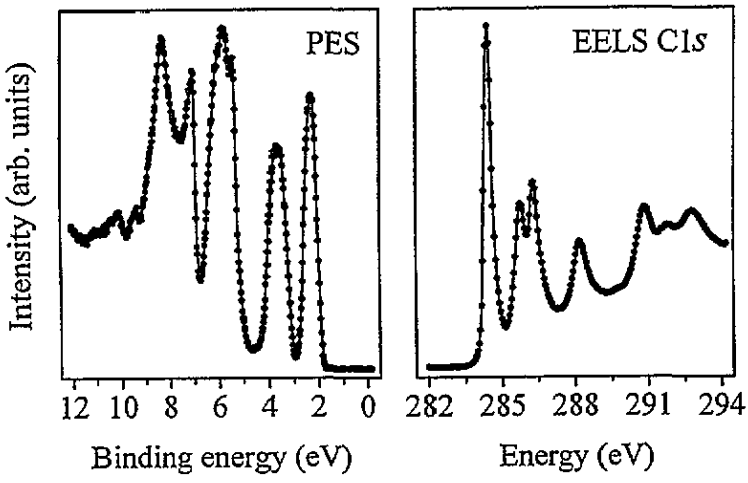

Figure 2. PES spectrum (left-hand panel, $h\nu = 21.22$ eV) and C 1s excitation spectrum (right-hand panel) of a thin film of C_{60}.

In the occupied states (see figure 2), the bands derived from the HOMO-1 (h_g, g_g) and HOMO-2 (t_{2u}, g_u) π MOs are centred at 3.7 and 5.8 eV binding energy (BE) respectively, with the lowest-energy feature at 2.3 eV being that derived from the HOMO (h_{1u}) MO. In analogy with other conjugated carbon systems [11], the structure in the C 1s excitation spectrum at energies below ~290 eV is attributed to transitions into bands derived from the unoccupied π^* MOs and the step-like structure at ~290 eV corresponds to the onset

of transitions into the unoccupied σ^* levels. Thus the leading peak in the C 1s excitation spectrum represents transitions into the empty band derived from the triply degenerate LUMO (t_{1u}) of C_{60}. The data shown in figure 2 are representative of C_{60} photoemission [48–52] and C 1s excitation spectra [50, 53] in the literature.

There have been many comparisons of the predicted electronic structure of fullerenes and fullerides with the results from experiment [35, 49, 50, 52]. The overall agreement is quite good, but there remain important discrepancies such as the underestimation of both the magnitude of the bandgap and the width of the bands derived from the HOMO and LUMO levels in the solid state. In addition, the predicted fine structure arising for example from the five h_{1u} subbands of the HOMO-derived feature is not observed in experiment [35]. As discussed in subsection 4.3, a significantly improved agreement with the experimental values of ~2.3 eV and ~1 eV for the $(N-1)\rightarrow(N+1)$ gap and HOMO bandwidth is achieved if the results of the GW calculation of Shirley and Louie are taken [33].

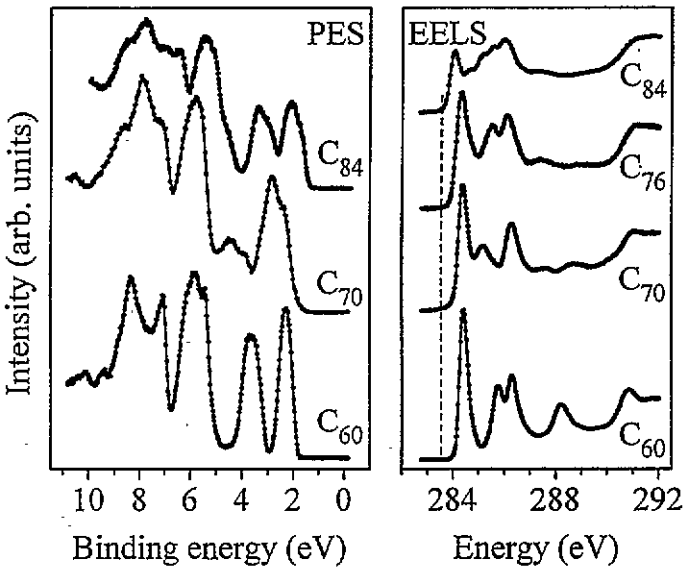

Figure 3. Left-hand panel, the PES spectra ($h\nu = 21.22$ eV) of solid C_{60}, C_{70} and C_{84}; right-hand panel, C 1s excitation spectra of thin films of C_{60}, C_{70}, C_{76} and C_{84}. The EELS data are normalized to the height of the C 1s $\rightarrow \sigma^*$ edge at ~290 eV. A dotted line in the right-hand panel marks the onset of the C_{84} spectral weight. The spectra are offset in the y direction.

PES measurements of the occupied electronic structure of C_{60} [35], C_{70} [55] and C_{84} [56] are shown in the left-hand panel of figure 3, and are representative of other data in the literature [57, 58]. The electron removal states located closest to E_F, at ~1.5–4 eV BE, are derived from the molecular HOMOs, together with some of the deeper-lying π^* MOs, (e.g. the HOMO-1 of C_{60}). This is followed by a group located at ~6 eV and a third lying deeper in energy between ~7 and 9 eV BE. The similarity of the gross features of the electronic structure from one fullerene to the next stems from their common molecular architecture. However, the spectra do differ, most noticeably in the first set of bands at lowest BE which results from the greater sensitivity of the highest-lying MOs to the details of the individual fullerene geometry and structure in the solid state. The lower molecular symmetry of the higher fullerenes is expressed in the reduced degeneracy of the molecular energy levels and thus an increased width of the observed bands in the PES spectra.

In the right-hand panel of figure 3, we show the C 1s excitation spectra of C_{60} [47], C_{70}

[47], C_{76} [59] and C_{84} [56]. The data are normalised to the σ^* step at ~290 eV, the height of which is roughly proportional to the number of carbon atoms in each fullerene. The data for C_{60} and C_{70} are similar to those from XAS [50, 53] and IPES [60]. It can be seen that as the fullerene size increases, the energy of the onset of the C 1s→π^* transitions decreases (as a guide to the eye, the onset of the C_{84} spectrum is denoted with a dotted line). This can be related to the decrease in curvature and concurrent decrease of C 2s character in the π electronic system (i.e. purer sp^2 bonding), as the larger fullerenes become more graphitic in nature [56, 59] The decrease in intensity of the first feature with increasing fullerene size, clearly signals the reducing degeneracy of the electronic structure near E_F which results from the lower symmetry of the higher fullerenes.

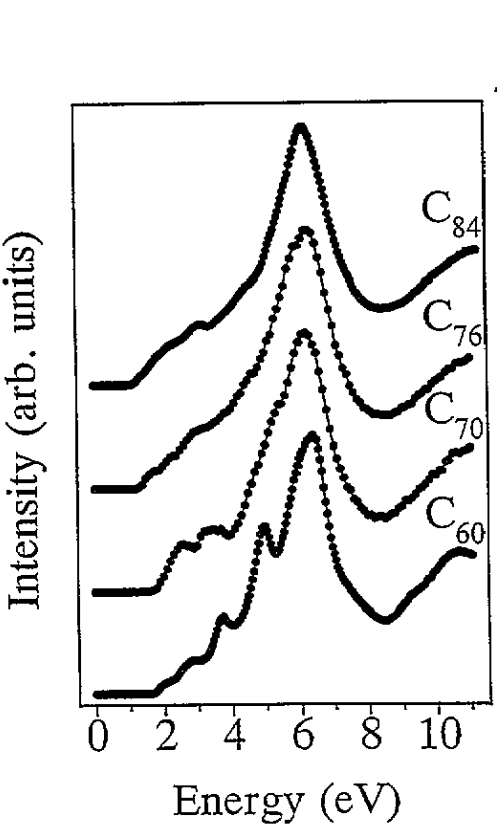

Figure 4. The loss functions of thin films of C_{60}, C_{70}, C_{76} and C_{84}. The data are normalized to have roughly equal π plasmon intensities and are offset in the y direction.

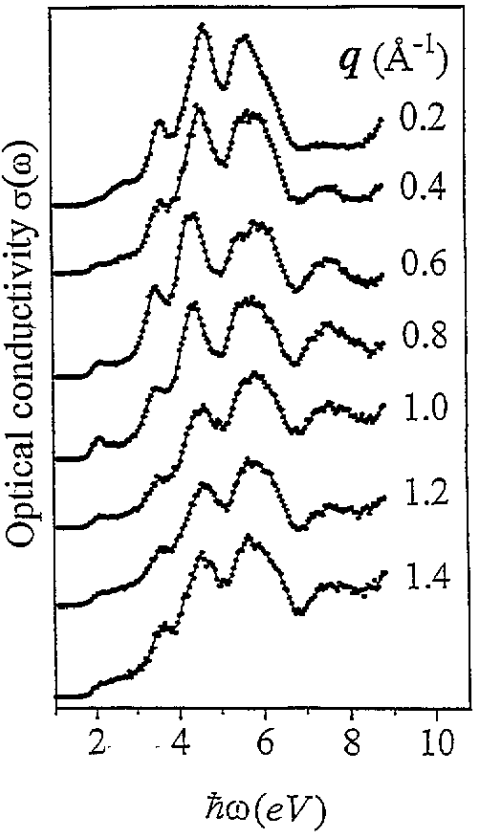

Figure 5. The optical conductivity, $\sigma(\omega)$, of a C_{60} thin film as a function of momentum transfer, q (q values in $Å^{-1}$ shown). The spectra are offset in the y direction.

Further information about the distribution of the π and π^* bands in the pristine fullerenes can be obtained from their valence level excitations. The loss functions for low momentum transfer ($q \sim 0.05$ $Å^{-1}$) of C_{60} [47], C_{70} [47], C_{76} [59] and C_{84} [56] are shown in figure 4. The general structure is familiar from studies of graphite [61] and conjugated polymers [11], in which transitions between the occupied and unoccupied π and π^*-derived states

give rise to peaks in the loss function, resulting in maxima centred at ~6 and ~25 eV which are often referred to as the π and $\pi+\sigma$ plasmon, respectively. The number of peaks due to $\pi \rightarrow \pi^*$ transitions resolved for C_{60}, and to a lesser extent for the higher fullerenes, is further evidence of the degree to which the molecular nature of the electronic structure of the fullerenes is retained in the solid state. The onset of the loss function decreases as fullerene size increases, from 1.8 eV for C_{60} to 1.2 eV for C_{84}. The loss functions shown in figure 4 can be used to derive ε_1 and ε_2 and hence the optical conductivity of each fullerene, showing the individual transitions between the π- and π^*-derived bands [47, 56, 59, 62].

EELS in transmission also allows measurement of the loss function as a function of momentum transfer, q. Figure 5 shows the optical conductivity, $\sigma(\omega)$, of C_{60} as a function of q up to 1.4 Å^{-1}, which has been derived from the loss function [63]. At low q, dipole-allowed transitions are favoured, but at high q these are suppressed in favour of monopole and quadrupole transitions. In figure 5, the intensity of a number of the features oscillates as a function of q. The transition responsible for the onset of the loss function at ~1.8 eV is non-dipole in character, as initially it is enhanced as q increases. In contrast those transitions giving rise to structure at ~2.4 and ~3.8 eV appear to be dipole allowed as initially their intensity falls off as q is increased.

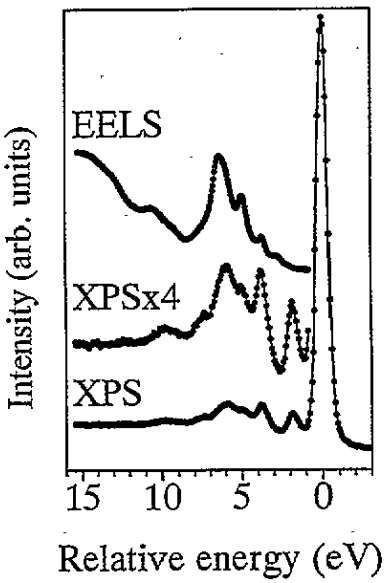

Figure 6. The C 1s core level photoemission spectrum of solid C_{60} measured with $h\nu = 400$ eV (labelled XPS). Shown for comparison are the same data multiplied by a factor of four in the y direction (labelled XPS × 4), and the loss function of C_{60} (labelled EELS, offset in the y direction). The energy is scaled relative to the C 1s BE of C_{60}.

Added insight into the character of the transitions between the π- and π^*-derived bands can be obtained from the intrinsic satellite structure observed in the C 1s core level photoemission spectrum of solid C_{60}. As was discussed earlier, photoemission gives a measure of the energy distribution of the electronic levels of the system in the ionized final state. Consequently it is possible to have final states in which the valence band electronic distribution is not that of the ground state, for example by excitation of an electron into one of the low-lying unoccupied levels. In such a situation, the energy of the final state is higher and so a satellite feature (sometimes called a 'shake-up') appears at higher BE in

the spectrum, separated from the main line by the energy of the valence band excitation. Figure 6 shows the C 1s core level photoemission spectrum of a thin film of C_{60} grown on GeS(001) recorded with 400 eV photons from the SRS, Daresbury Laboratory (UK) [55]. In agreement with previous studies [52, 64], the main part of the spectrum consists of a single, symmetric peak located at a binding energy of ~285 eV. The FWHM of 780 meV is resolution limited. The satellite structure at higher BE is is also shown, amplified by a factor of four, together with the loss function of solid C_{60} (as shown in figure 4). Satellite structures are visible at separations of 1.9, 3.8, ~4.9, 5.9, ~7.6, and 9.6 eV from the main C 1s core line. Many of the features in the PES spectrum have analogues in the loss function, and thus can be assigned to the excitation of $\pi \rightarrow \pi^*$ transitions. It is interesting to compare the relative intensities of the features in the EELS spectrum (which picks out dipole transitions) and those from the shake-up process (which allows monopole transitions) [9]. The most obvious intensity differences are between the π plasmon excitation at 6 eV (which is more intense in EELS), and the 1.9 eV feature which is strongly favoured in the shake-up spectrum. This also suggests that the transition responsible for the 1.8 eV onset seen in the loss function measured by EELS is monopolar in character. In EELS conducted with these high primary beam energies, this transition is in fact a singlet exciton, in which an electron has been excited from the HOMO- to the LUMO-derived levels of the same C_{60} molecule in the solid. The corresponding triplet exciton is observed at ~1.5 eV in EELS in reflection [65] and solid state optical absorption data [66]. The fact that the onset of the optical absorption spectrum of C_{60} in solution is also about 1.5 eV [67], adds weight to the argument that the 'gap' transitions observed in EELS and optics correspond to the formation of a Frenkel exciton (a charge neutral excitation) [34]. The true transport gap of solid C_{60}—the energy required to remove an electron from one C_{60} molecule and put in onto a second, widely separated, molecule—is given by the separation of the onsets of the PES and IPES spectra, which is ~2.3 eV (onset to onset) or ~3.5 eV (HOMO peak to LUMO peak) [9, 34, 54, 68] As was discussed in subsection 4.4, U for two holes located on the same C_{60} molecule is of the order of 1.5 eV. It is this relatively large value of U in comparison to the bandwidth which results in exciton formation, and means that the energy penalty paid for the creation of separate $(N-1)$ and $(N+1)$ states is not equal to the simple splitting in energy between the highest occupied and lowest unoccupied MOs. The distinction between electron removal (e.g. h_{1u}-derived states in C_{60}) and electron addition (e.g. t_{1u}-derived states in C_{60}) states is clearly seen from the separation of the h_{1u} and t_{1u} levels of K_6C_{60} in the solid state (see figure 8) which is ~1.7 eV [35], as both of these levels are now electron removal states (although the non-rigid band-like changes of the electronic structure upon intercalation also play a role here).

Excitons also play a role in the low-energy excitation spectra of the higher fullerenes. In figure 4 shown above, for each of the fullerenes measured, the gap from EELS in the solid state is also similar to that observed in solution, and is significantly smaller than the transport gap derived from PES/IPES data. From the difference between the EELS and PES/IPES gap values, the exciton binding energy can be estimated to be ~0.5–0.8 eV for C_{60}, C_{70} and C_{84} [59].

The preceding discussion highlights the tendency of solid C_{60} and other fullerenes to behave in a localized, molecular manner. In addition, the prediction that despite the orientational disorder, K_3C_{60} does support extended, band-like electronic states should be tested [32]. One test of this is the observation, or otherwise, of band dispersion in C_{60} using ARPES (as the preparation of single crystals of K_3C_{60} suitable for ARPES measurements has yet to be mastered). LDA quasiparticle calculations predict a dispersion of the HOMO-derived bands of ~0.9 eV [33], with conventional LDA calculations predicting a dispersion

of ~0.9 eV for the (HOMO-1)-derived bands [8, 69]. Consequently measurement of dispersion of this order by ARPES would normally be expected to be well within the grasp of the present state of the art photoemission instrumentation.

Until lately, the existing experimental evidence from angle-resolved studies pointed towards small or negligible dispersion of the occupied [70] and unoccupied [71] bands of C_{60}. Recently, a number of ARPES experiments on the $C_{60}(111)$ surface have been published [55, 72, 73]. In the first, photoemission carried out with $h\nu = 29$ eV showed few signs of dispersive behaviour in either the HOMO- or (HOMO-1)-derived bands, but with $h\nu = 8.1$ eV revealed significant structure in the HOMO-derived band [72]. This structure was interpreted in terms of two main components, one which remains relatively constant in energy and one which disperses by ~400 meV along the $\overline{\Gamma}$–$\overline{K}$ direction of the surface Brillouin zone (SBZ). The dispersive feature is accompanied by two vibronic sidebands each separated by ~200 meV, thus leading to the observed HOMO band width of ~1 eV. The difference between the data recorded with $h\nu = 29$ and 8.1 eV was attributed to the improved k-resolution achieved using lower photon energy. However, photoemission with photon energies as low as 8 eV no longer gives information solely on the initial DOS, but rather on the energy distribution of the joint (initial *and* final) density of states. Therefore the fine structure observed with $h\nu = 8.1$ eV could also result from either strong modulations in the cross-section for photoemission from the five underlying HOMO subbands into the highly structured final states only a few electron volts above E_F, or dispersion of the final states themselves. In an attempt to resolve this question, we carried out high-resolution ARPES experiments with a photon energy ($h\nu = 16.8$ eV) intermediate between those used in [72]. The data are shown in figure 7. No large angle-dependent changes are observed in the HOMO-derived manifold, but distinct changes are observed in the HOMO-1, with a shoulder gradually dispersing to higher BE than the main band on scanning along the $\overline{\Gamma}$–$\overline{K}$–$\overline{M}$ high-symmetry direction of the $C_{60}(111)$ SBZ [55, 74]. Although the momentum resolution conferred by the higher final state energy is inferior to that at $h\nu < 10$ eV, the gradual changes in the HOMO-1 feature as a function of $k_{\|}$ suggest dispersion in either the initial and/or final states as the underlying cause of the angle-dependent spectral structure. However, the small size and three dimensionality of the Brillouin zone of C_{60}, together with the multiband nature of both the HOMO and HOMO-1 features, make it impossible to assign a particular feature in the EDCs to a corresponding subband in the bandstructure [74]. A similar conclusion was arrived at recently in a thorough ARPES study of $C_{60}(111)$ conducted with $8.1 < h\nu < 10.8$ eV [73]. Here, the role of the final DOS was clearly shown, with features observed in both the HOMO and HOMO-1 spectra due to photoemission into a final state ~6.2 eV above E_F which shows dispersion of ~0.6 eV on going from $\overline{\Gamma}$ to $\overline{M}$ [73]. For photoemission at normal emission with $h\nu = 9$ eV, the width of the HOMO-1 feature in [73] was only ~0.6 eV, which on comparison with the width of ~1 eV observed in gas phase PES spectra [75], led the authors to discount vibronic losses as a major contribution to the observed bandwidth in photoemission of solid C_{60} [73].

6. High-energy spectroscopic results from fullerides

In the second half of this article, we will discuss the electronic structure of fullerides from the point of view of high-energy spectroscopies. Fulleride is the term coined for the generally ionic compounds formed on intercalation of fullerenes with the alkali and alkaline-earth metals [76]. In the following, we use the A_xC_{60} (A = K, Rb and Ca) and A_xC_{70} (A = Rb) systems as examples with which to relate the present understanding of fulleride electronic structure and highlight some of the current issues in this field.

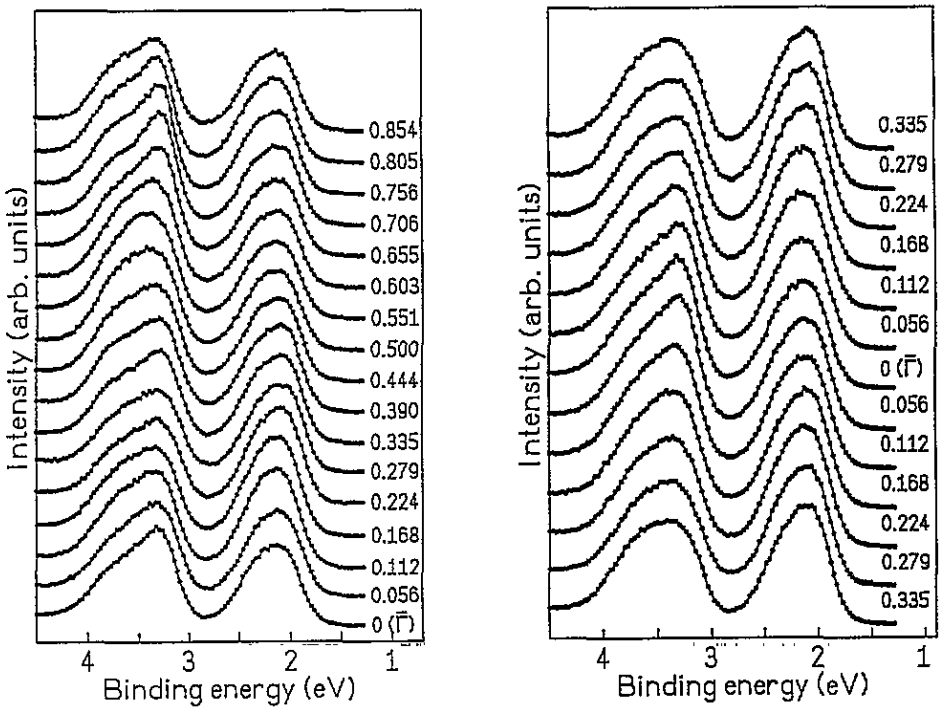

Figure 7. Angle-resolved PES EDCs of the HOMO- and (HOMO-1)-derived bands of solid C_{60} recorded with $h\nu = 16.8$ eV. The values of $k_{\parallel}$ (in $Å^{-1}$) for photoemission from the HOMO-derived band are indicated. The left-hand panel shows spectra recorded in the $\bar{\Gamma}$–$\bar{K}$–$\bar{M}$ direction, and the right-hand panel those in the $\bar{M}$–$\bar{\Gamma}$–$\bar{M}$ direction in the $C_{60}(111)$ SBZ.

6.1. The alkali metal C_{60} fullerides, A_xC_{60}

Before discussing the data from the A_xC_{60} materials in detail, it is worthwhile to briefly consider the issue of the stoichiometry of fulleride samples studied using high-energy spectroscopy. In a typical high-energy spectroscopic study of a fulleride system, it is no easy task to precisely determine the doping value, x, and the phase or phases present in the sample under investigation, the exception being the saturated A_6C_{60} (A = K, Rb, Cs) phases. As far as the global stoichiometry is concerned, core level PES (XPS) measurements, if available, represent the best method for determining (within an accuracy of 10%) the A/C ratio pertinent to the near surface layer probed by the valence band PES. This method has been used by many groups [9, 35, 37, 77]. It has been proposed [78] that, due to its surface sensitivity, PES measurements represent the superposition of bulk and surface spectra, the latter due to the differing K coordination of the C_{60} molecules at the surface. An additional quantification method involves the analysis of the integrated area of the fullerene LUMO-derived spectral weight normalized to the area of the HOMO (or HOMO plus HOMO+1), using either XPS/XAS measurements as a calibration, or the assumption that intercalation stops at $x = 6$ [9, 35, 50, 79–82]. A further option is to study the electrical conductivity of a test film grown in parallel to that under investigation, assuming, for example, that the conductivity is a maximum for A_3C_{60} (A = K, Rb) [51, 68, 81]. This method suffers from the drawbacks that the conductivity measurement is usually not carried out on the same sample that is investigated using high-energy spectroscopy, and that the probing depths of the two experiments can be very different. Some of the discrepancies between the high-

energy spectroscopic data in the literature, and the debate these have raised, can be traced back to differences in the intercalation stage between the samples studied in the different laboratories, despite a common x value designated by the authors in each case. In addition, it has long been realized that the growth of fulleride thin films under UHV conditions may represent conditions far from equilibrium, for example resulting in K_4C_{60} formation in a film whose global stoichiometry lies below $x = 3$ [83]. This can mean that the global stoichiometry of the fulleride film does not in itself designate the phase(s) present in the sample. (Phase-related information can however be gathered from the analysis of the K 2p XPS lineshape, which allows the determination of the relative number of K^+ ions occupying the tetrahedral and octahedral interstitial sites of the C_{60} host lattice [84]. This technique has been exploited to derive a phase diagram for the K–C_{60} and K–C_{70} systems [16, 85, 86].)

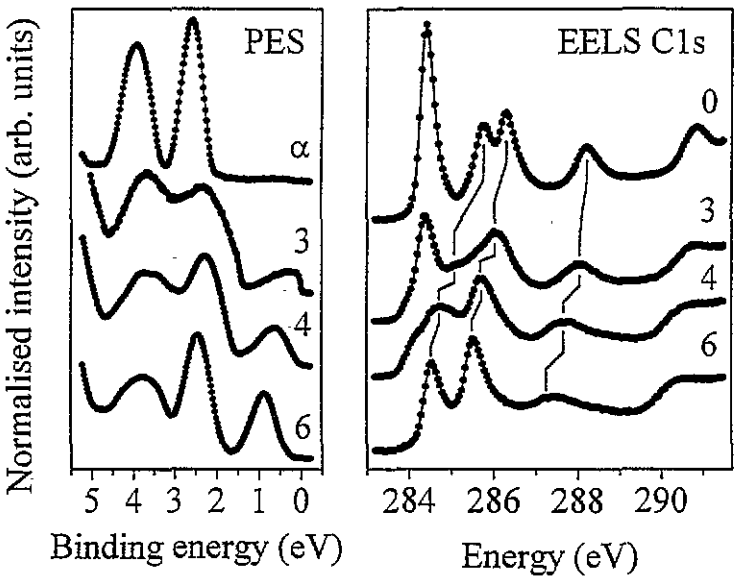

Figure 8. PES spectra (left-hand panel, $h\upsilon = 21.22$ eV) and C 1s excitation spectra (right-hand panel) of K_xC_{60}, with x values as shown. For 'α', $x \sim 0$ (see text). All spectra are recorded at room temperature. Data are normalized to the HOMO spectral weight and C 1s $\rightarrow \sigma^*$ step for PES and EELS, respectively, and are offset in the y direction. The connecting lines drawn in the right-hand panel show the changing energy positions of the features in the unoccupied electronic structure upon K intercalation.

Thus the photoemission data of C_{60}, K_3C_{60}, K_4C_{60} and K_6C_{60} shown in the left-hand panel of figure 8 are representative of the phases indicated, but for the reasons outlined above do not necessarily correspond to an overall sample stoichiometry of exactly $x = 3$, 4 and 6. The spectrum labelled α-C_{60} was recorded from a sample which had been exposed to a very low flux of K atoms, which results in a highly dilute solid solution of K^+ in C_{60}. The Fermi level in this case is pinned at donor levels at the base of the LUMO-derived bands, thus causing a shift of the spectrum to higher BE in comparison to the spectrum of pristine C_{60} shown in figure 3. For K_3C_{60}, the charge transfer of three electrons to C_{60} is clearly signalled by the presence of a new feature located in the former gap. This is the half-filled band formed from the triply degenerate molecular (t_{1u}) LUMO. On further intercalation to $x \sim 4$ the LUMO-derived peak has grown further and shifted away from E_F, resulting in small or zero intensity at E_F. By $x = 6$ the LUMO-derived band is completely full and

there is a clear gap between the highest occupied (t_{1u}) states and E_F. For samples prepared in this manner (see section 3), no unique spectral signature of KC_{60} is found at room temperature and spectra for samples with $0 < x < 3$ can be synthesised from the sum of the appropriately weighted spectra of α-C_{60} and K_3C_{60} [28, 35]. Phase separation at or below room temperature between C_{60} and K_3C_{60} for $x \leqslant 3$ has also been observed in a number of other experiments such as x-ray diffraction [6], NMR [87], Raman [88] and infrared spectroscopy [89]. However, recent work suggests that different preparation conditions can result in the formation of KC_{60}. At elevated temperature, AC_{60} (A = K, Rb Cs) is fcc with the alkali metal ion situated in the octahedral site (rock-salt structure) [21]. On slow cooling, an orthorhombic structure is formed with an unusually short intermolecular distance along the crystallographic a direction [90]. These orthopolymers are (unusual) metals at room temperature, and show a transition to a spin density wave (SDW) state below ~90 K [22, 9].

The right-hand panel of figure 8 shows the C 1s core level excitation spectra of the same systems [47, 92]. The samples for EELS measurements were ~1500 Å thick, the K_3C_{60} and K_4C_{60} samples being prepared by vacuum distillation. *In situ* electron diffraction measurements could further confirm the phase purity of the fcc K_3C_{60} [93], bct K_4C_{60} [94] and bcc K_6C_{60} [47] samples. As in figure 3, the spectra are normalized to the height of the C $1s \rightarrow \sigma^*$ step at ~290 eV. The uppermost spectrum (pristine C_{60}) has been discussed earlier, and shows structures due to transitions into the bands derived from π^* molecular orbitals of C_{60}. The first feature, due to C $1s \rightarrow t_{1u}$ (C_{60} LUMO) transitions, decreases in intensity by 50% on going from C_{60} to K_3C_{60}, as would be expected for half filling of the LUMO-derived band. For K_4C_{60}, its intensity is additionally reduced, consistent with *further charge transfer to* C_{60}. *In* K_6C_{60}, *this feature is no longer visible, as the* t_{1u} *band* is completely filled [47] and is therefore seen to lie completely below the Fermi level in the PES spectrum. Thus the first peak represents instead transitions into states derived from the molecular t_{1g} level, as is illustrated by the connecting guide lines drawn in the figure. The second peak corresponds to transitions into states derived from the molecular h_g level. The shift to lower energy and the broadening apparent in the spectra of the fullerides both show the relaxation of the electronic structure of C_{60} on intercalation, as well as the charge-transfer-induced chemical shift of the core level.

It is clear from figure 8 that a relatively straightforward picture of the electronic structure of C_{60} and K_6C_{60} suffices, with gaps between the occupied and unoccupied electronic levels as expected, albeit the magnitude of which may well reflect a strong on-site Coulomb repulsion energy. However, it is in the intermediate regime that things become more complex. In the following we discuss the PES and EELS spectra of the A_3C_{60} materials in some detail, with particular reference to the alternative interpretations of their t_{1u}-derived spectral weight measured in photoemission. We then close the section devoted to alkali metal fullerides with a discussion of the high-energy spectroscopic data from the A_4C_{60} materials.

PES data [35, 50, 77, 95, 96], as well as conductivity measurements of K_xC_{60} prepared in vacuo [36, 97, 98] attest to the metallic nature of a phase in thin-film samples with x equal or close to three. However, as was discussed in subsection 4.4, the magnitude of U in solid C_{60} has lead to the suggestion that stoichiometric K_3C_{60} has a gap of ~0.7 eV, with the metallic and superconducting phase being off stoichiometric [34]. Nonetheless, the convergence of most of the experimental data to date towards integral K content does not allow a large deviation from $x = 3.0$. If, for the sake of argument, we set aside the debate over the exact stoichiometry of the A_3C_{60} superconductors, it is interesting to examine to what extent the independent-particle picture is successful in the detailed

description of the high-energy spectroscopic data from the A_3C_{60} systems. It can be seen from the data of figure 8 that the description of K_3C_{60}'s electron removal (PES) and electron addition [99] spectra in terms of a rigid shift of the Fermi level through the DOS predicted within the independent-particle approximation is not very accurate. Quite apart from the relatively constant BE position of the peak representing the occupied h_u (HOMO) states of C_{60} through the K_xC_{60} PES series and the changing relative energies of the unoccupied bands as a function of intercalation, the departures from the rigid-band description are most easily seen in the t_{1u}-derived spectral weight. LDA quasiparticle calculations predict a total t_{1u} bandwidth of ~0.7 eV for K_3C_{60} [33]. Thus one would expect an occupied part of this band of width 0.35 eV appearing in the PES spectra. The width of the occupied part of the t_{1u} spectral weight seen in PES is ~1.2 eV, and so when one considers in addition the unoccupied part, it becomes rapidly clear that something is resulting in a redistribution of the t_{1u} spectral weight.

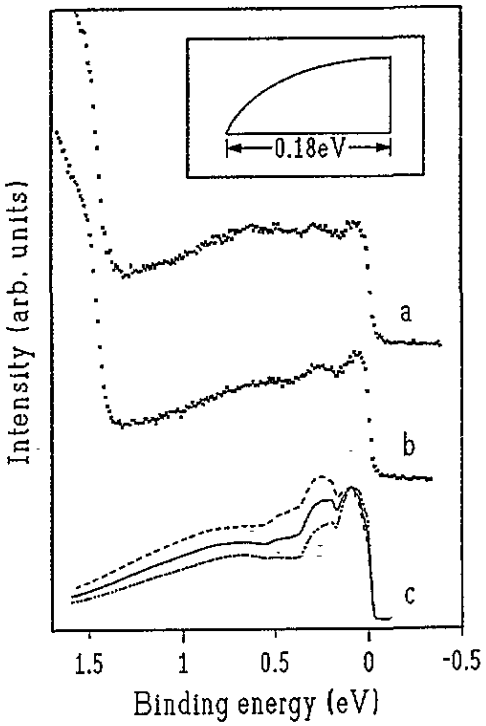

Figure 9. Photoemission spectral weight of (a) K_3C_{60} and (b) Rb_3C_{60} t_{1u}-derived bands recorded at $T = 10$ K using $h\nu = 21.22$ eV. Also shown in (c) are calculated PES spectra of A_3C_{60} (A = K or Rb) with electron–phonon coupling constants, $\lambda/N(0)$, of 0.068 (dotted–dashed line), 0.095 (solid line) and 0.112 (dashed line). (See [100].) The inset shows the form of the half-filled conduction band used in the calculation.

A clue as to what may be partly responsible for the anomalous width of the t_{1u} spectral weight can be gained from the high-resolution photoemission measurements of K_3C_{60} and Rb_3C_{60} at low temperature shown in figure 9, in which fine structure becomes visible comprising a peak at E_F followed by a second peak located some 250 meV to higher BE, with a broader feature centred at ~600 meV. Similar data have been recorded for K_3C_{60} by Benning *et al* [95]. The structures near E_F ($0 < \mathrm{BE} < 300$ meV) are generally agreed to be phonon satellites, resulting from the excitation of molecular vibrons during the

photoemission process [95], in analogy to the phonon sidebands observed in the PES of gas phase C_{60}^- [46]. Also shown in figure 9 are PES profiles of A_3C_{60} calculated within a model [100] which shows that good agreement can be found by taking into account relatively strong coupling of the electronic system to the molecular Ag and Hg modes ($\lambda/N(0) = 0.095$), together with coupling to the charge carrier plasmon observed at ~0.5 eV in EELS studies. An alternative interpretation of the PES intensity at higher energies has been proposed in terms of a shift of spectral weight due to the effects of correlation [95], in which it is suggested that K_3C_{60} could lie in the region of U/W in which a remnant of the lower Hubbard band remains in the electron removal spectrum, despite the clear metallic nature of the carriers close to E_F [101]. Calculations of the electron removal spectrum of off-stoichiometric $K_{3\pm\delta}C_{60}$ within a localized degenerate Hubbard model are able to reproduce satellite structure at higher energies, in both the t_{1u}- and h_g-derived spectral weight [39]. However, for good agreement with the experimental PES spectra both a non-stoichiometry of $\delta \geqslant \pm 0.4$ and a value of $U = 0.7$ are required. This non-stoichiometry is outside the range of the commonly agreed error bars in the XPS analysis used to determine the sample stoichiometry in the PES experiments. Perhaps more importantly, $U = 0.7$ eV is about one-half of the value determined experimentally for C_{60} and K_6C_{60} [34, 37]. Direct determination of U in K_3C_{60} by comparison of Auger and PES spectra is complicated by intermolecular screening of the core hole in the Auger initial state leading to a shift of the Auger spectrum. It has however been concluded that U should be of the same magnitude as in C_{60} and K_6C_{60} [37]

Figure 10 shows high-resolution PES measurements of the t_{1u}-derived spectral weight of K_3C_{60} recorded as a function of temperature between 15 and 425 K [102]. Similar results have also been observed for Rb_3C_{60} [100]. The smearing out of the fine structure and reduction of the intensity at E_F observed as the temperature is increased is greater than can be accounted for by simple thermal broadening. The calculated PES profile, using the same method as gave a good fit for the low-temperature spectrum in figure 9, is shown as a solid line superimposed upon the $T = 425$ K PES spectrum. The calculation takes into account the broader Fermi–Dirac distribution at this temperature as well any changes in the population of the C_{60} molecular vibrations, but is still clearly unable to account for the observed transfer of spectral weight to higher energies. The gradual change in spectral profile across the whole temperature range and the similarity in the behaviour of both K_3C_{60} and Rb_3C_{60} argues against phase transitions as a cause. It remains an open question as to whether coupling to either low-energy anharmonic alkali metal optical phonons or librations or a disorder-driven transition from a metallic to a localized state may play a role in the observed temperature dependence of the t_{1u}-derived spectral weight.

Further insight into the evolution of the electronic structure of C_{60} as a function of alkali metal intercalation is possible from the study of the valence band excitations of the fullerides. Figure 11 shows the loss functions for low momentum transfer of of C_{60}, K_3C_{60}, K_4C_{60} and K_6C_{60} [47, 92]. The samples are the same as those from which the C 1s excitation data of figure 8 were recorded. The energy range displayed (up to 2 eV) contains only features related to the low-energy intraband and interband ($\pi \rightarrow \pi^*$) excitations—the higher-energy features of the K_xC_{60} loss function are similar to that of C_{60} with π and ($\pi + \sigma$) plasmons located at ~6 and 25 eV, respectively [47]. The clear gap in the valence band excitation spectra of C_{60} at low-energy (figure 11) points once again to its insulating nature, with the dipole-forbidden, excitonic gap transition giving rise to the weak spectral structure at ~1.8 eV (see section 5 above). In comparison with C_{60}, the loss function of K_3C_{60} in this energy region contains two new low-energy features. The first, located at ~0.55 eV, is a combination of the plasmon associated with the charge carriers occupying the half-filled t_{1u}

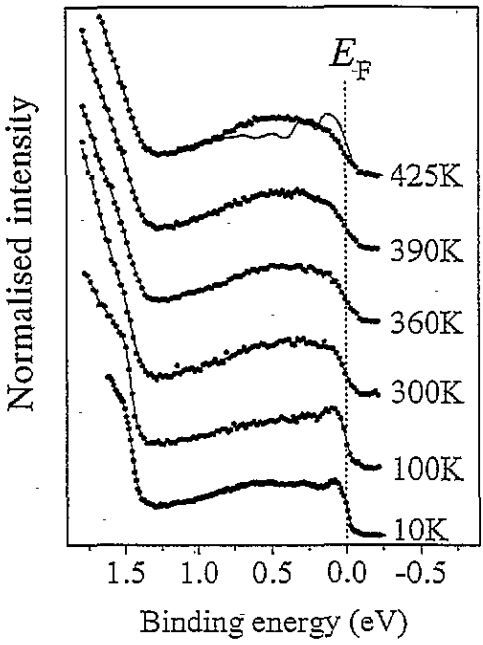

Figure 10. The t_{1u}-derived photoemission spectral weight of K_3C_{60} as a function of temperature, recorded with $h\upsilon = 21.22$ eV. The position of the Fermi level is marked with a dotted line. The solid line superimposed on the $T = 425$ K experimental spectrum is the calculated PES profile for this temperature (see the text). The spectra are offset in the y direction.

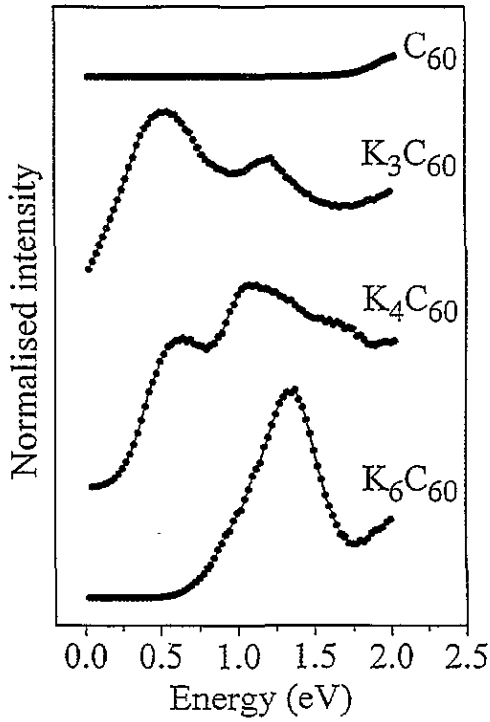

Figure 11. The loss function of K_xC_{60} ($x = 0$, 3, 4 and 6). The data are normalized to the intensity of the π plasmon located at ~6 eV and offset in the y direction.

conduction bands and transitions within the three t_{1u} subbands themselves [93]. The second new feature at ~1.2 eV, is related to the transition from the now partially filled t_{1u} bands into the unoccupied t_{1g} (C_{60} LUMO+1) bands. EELS in transmission measurements also allow the study of the 0.55 eV plasmon in K_3C_{60} as a function of momentum transfer, q. Recently it was proposed that as a consequence of the high degree of localization of the charge carriers on the C_{60} molecular units, the plasmon dispersion should be negative in q [103]. This is not what would be expected for a simple free-electron metal, in which a positive quadratic plasmon dispersion is observed, in agreement with the predictions of calculations carried out within the random phase approximation (RPA) [104]. Figure 12 shows the loss function of K_3C_{60} in the region of the charge carrier plasmon measured across a q range of more than 0.5 $Å^{-1}$ (which is greater than the K_3C_{60} Brillouin zone dimension of ~0.44 $Å^{-1}$) [102, 105]. The measured energy position of the plasmon does not change within experimental uncertainty. This can be understood in terms of the interplay between the local field corrections to RPA which lead to negative dispersion (as pointed out by the authors of [103]), and the reduced screening of the plasmon at higher q due to the background dielectric function resulting from interband transitions [105]. This screening appears to almost exactly offset the local field effects resulting in the observed lack of

dispersion [105].

The loss function of K_6C_{60} is more straightforward, with a single asymmetric peak located at ~1.35 eV resulting from $t_{1u}t_{1g}$ interband transitions [47, 94]. For low momentum transfer, the intensity of this first feature in K_6C_{60} is significantly greater than that of the C_{60} gap transition, as in the fulleride the gap transition is dipole allowed. The loss functions recorded from other A_6C_{60} fullerides (A = Na, Rb, Cs) are very similar to that of K_6C_{60} [47], attesting to the relative lack of perturbation of the C_{60} molecular orbital degeneracy in the A_6C_{60} fullerides.

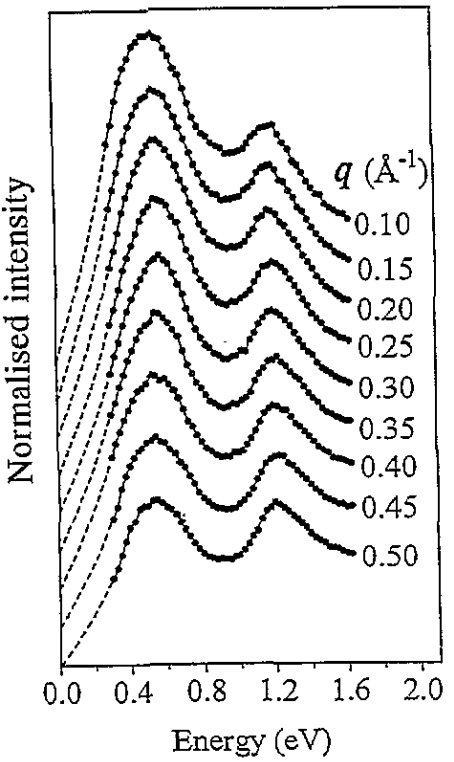

Figure 12. The q-dependence of the loss function of K_3C_{60} in the region of the charge carrier plasmon ($E \sim 0.5$ eV) and the peak related to $t_{1u} \rightarrow t_{1g}$ interband transitions ($E \sim 1.2$ eV). The values of the momentum transfer (in $Å^{-1}$) are shown and the spectra are offset in the y direction.

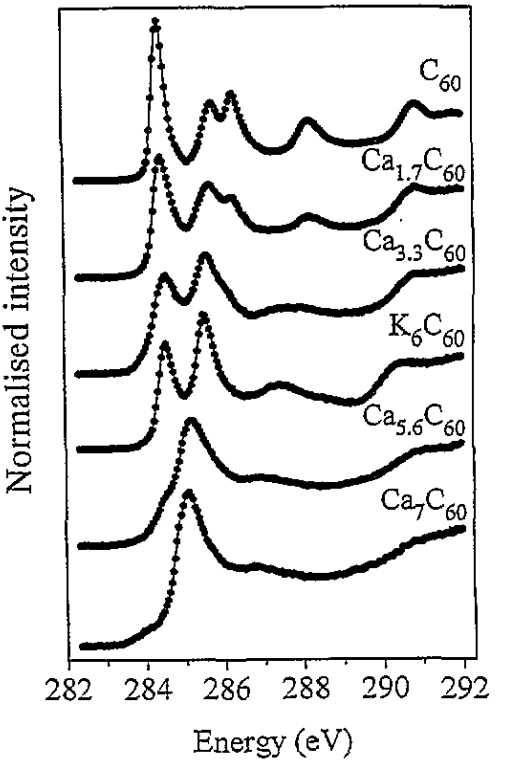

Figure 13. C 1s excitation spectra of Ca_xC_{60} ($x \sim 0$, 1.7, 3.3, 5.6 and 7) and K_6C_{60}. The data are normalized to the height of the C 1s $\rightarrow \sigma^*$ edge at ~290 eV and offset in the y direction.

From the preceding discussion it is clear that the simplest picture in which fullerides with partially filled bands are metallic, with the conduction band electronic structure determined by the position of the Fermi level in the t_{1u} DOS is insufficient to account for the details of the electron removal and electron addition spectra of the A_3C_{60} materials. We now progress to the discussion of the A_4C_{60} (A = K, Rb, Cs) materials—which also contrary to the simple model outlined above are non-metals [95, 97, 106, 107]. Despite the fact that the failure of these materials to show metallic behaviour is potentially as interesting (although not as glamorous) as the superconductivity observed in the intensively studied

A_3C_{60} fullerides, there have been few studies dedicated to the electronic properties of A_4C_{60} [27, 97, 106]. In thin-film conductivity studies it has been found that 'back- doping' from A_6C_{60} by addition of C_{60} readily produces a recognisable A_4C_{60} signature, whereas doping 'forwards' from $x \sim 3$ tends to result in a less clear-cut A_4C_{60} phase [36]. This observation can be understood as a result of the body-centred (cubic) structure of A_6C_{60} forming a better template for bct A_4C_{60} formation than does fcc A_3C_{60}. One result of this was the ease with which it was possible to 'miss' the A_4C_{60} phase in, for example, PES investigations with intercalation carried out in the 'forward' direction [108]. A still better method for the production of phase-pure A_4C_{60} material is vacuum distillation (see section 3). With the benefit of hindsight, or vacuum distillation, it is now a relatively straightforward task to produce a more or less phase pure A_4C_{60}. As regards electronic structure, it is clear from the data shown in figures 8–11 that in the case of K_4C_{60} the simple picture of fulleride electronic structure breaks down completely. The photoemission spectrum (figure 8) shows zero or close to zero DOS at E_F, consistent with the non-metallicity of K_4C_{60}, despite the nominally partially filled t_{1u} band [106]. In the C 1s excitation spectrum, the peaks representing C 1s$\rightarrow t_{1g}$ and C 1s$\rightarrow h_g$ transitions appear to be broader than in K_6C_{60} (which is also non-metallic, and so the lifetime and core excitonic effects would be expected to be similar). The loss function shown in figure 11 provides evidence that the electronic states of K_4C_{60} close to E_F are split, and it is this splitting which is responsible for the broadening in the C 1s excitation spectrum and the lack of intensity at E_F in the photoemission. The other A_4C_{60} fullerides have similar loss functions, although the spectral structure seems to become sharper on going from A = Na $\rightarrow$ K $\rightarrow$ Rb $\rightarrow$ Cs, which may result from the larger number of nearest neighbours in the fcc Na_4C_{60}, and the increasing lattice constant as the alkali metal radius increases—thus leading to a decreased overlap of the C_{60} molecular orbitals [94]. The splitting makes itself clear in figure 11 as the appearance of a number of extra features in the loss function, in place of the excitations between the t_{1u}- and t_{1g}-derived levels that appear at 1.4 eV for K_6C_{60}. New features are observable at 0.65, 1.1 and 1.65 eV for K_4C_{60}. As K_4C_{60} is an insulator, these new features must be due either to transitions between states derived from the t_{1u} levels, or between states derived from the filled t_{1u} and empty t_{1g} levels. In a simple picture, the remnants of the former C_{60} gap transition ($h_g \rightarrow t_{1u}$) would appear at ~1.8 eV, as in C_{60} itself, and all other possible transitions between more widely separated electronic levels would lie to higher energy. At the time of writing, it is not completely clear what is responsible for the splitting of the electronic levels near E_F (i.e. the lowering of the degeneracy) in the A_4C_{60} materials, possible candidates however, being the effects of electron correlation [38], electron–phonon coupling expressed as a Jahn–Teller splitting of the electronic levels around E_F [44, 45], or the formation of a spin or charge density wave [109]. As discussed earlier (subsection 4.5), Jahn–Teller effects are agreed to be important for the $(C_{60})^{n-}$ molecule [46], although to what extent they would survive solid formation is unclear at present. The Jahn–Teller picture in the solid state does however gain support from the observation of satellites due to electron–phonon coupling observed in the PES spectra of K_3C_{60} [95, 100] (see figure 9) and $(C_{60})^{\sim 3-}$ molecules adsorbed upon the K/Au(110)c(2 × 2) surface [110].

6.2. *The alkaline-earth fullerides: Ca_xC_{60} and Ba_xC_{60}*

The electronic structure of some of the alkaline-earth-intercalated fullerides has also been investigated using high-energy spectroscopy. Following the discovery of superconductivity in Ca_5C_{60} [111] and Ba_6C_{60} [112], these compounds have been the most widely investigated. For both of the superconducting compositions, hybridization has been predicted between

the alkaline-earth levels and those of the fullerene from LDA bandstructure calculations [113–115]. In other words, the assumption of total charge transfer from guest to host can no longer be made. The accuracy of this prediction has been borne out in PES studies of the AE_xC_{60} (AE = Ca and Ba) systems, in which intercalation beyond $x \sim 3$ results in the appearance of alkaline-earth electronic states in the occupied electronic structure within a few electron volts of E_F [113, 116, 117]. These AE-derived states have been observed either by recording the PES EDCs at higher photon energies (e.g. with Al $K\alpha$ x-rays), at which stage the photoionization cross-section greatly favours emission from the AE-derived electronic states [113, 116], or, in the case of Ba_xC_{60}, using resonant photoemission at the Ba 4d threshold to highlight the Ba-related spectral structures [117]. Despite the hybridization, at higher intercalation levels such as those in the superconducting compositions, enough charge is transferred from the alkaline-earth atoms to populate the band derived from the C_{60} t_{1g} MOs (i.e. the LUMO+1 of C_{60}).

In such cases, the study of core level excitation spectra has the advantage that it allows the site specific estimation of the degree of charge transfer in the alkaline-earth fullerides. Figure 13 shows the C 1s excitation spectra of Ca_xC_{60} together with that of K_6C_{60} [118]. The reduction in intensity of the first feature with increasing Ca content clearly signals the charge transfer from Ca on successive intercalation. The C 1s excitation spectrum of $Ca_{3.3}C_{60}$ closely resembles that of K_6C_{60}, in which six electrons have been transferred to the fullerene host's t_{1u}-derived band, which is then located fully below E_F (and so not seen in the C 1s excitation spectrum). For $Ca_{5.6}C_{60}$ the t_{1u}-derived feature is absent as expected, but the intensity of the next t_{1g}-related feature is also significantly reduced. On further intercalation to $x \sim 7$, the t_{1g} spectral weight is still smaller, and one can roughly estimate a C_{60} charge state in Ca_7C_{60} of $\sim 11-$, clearly showing the reduced degree of charge transfer from the Ca at higher intercalation levels. Charge states greater than 6− have also been observed in PES studies of C_{60} molecules deposited in submonolayer coverages upon alkali metal films held at low temperature—one group [107] reporting maximum possible charge states of $(C_{60})^{8-}$ and others [110, 119] $(C_{60})^{12-}$ for C_{60} on thick K films. The significant point in the case of the Ca and Ba fulleride superconductors is that the electronic states at E_F responsible for superconductivity are located in a different band (t_{1g} derived) than those in the alkali metal A_3C_{60} superconductors (t_{1u} derived).

6.3. Higher fullerene intercalation compounds (e.g. Rb_xC_{70}) and endohedral fullerenes

In analogy with the C_{60} fullerides, intercalation compounds can also be formed between the higher fullerenes and metals. Due mainly to supply, A_xC_{70} has been the focus of most spectroscopic attention in this area [16, 47, 120, 121], although A_xC_{76} [122], A_xC_{82}, [82] A_xC_{84} [64, 123] and A_xC_{96} [124] have also been studied by high-energy spectroscopy, mostly for A = K. In this final section, we use EELS and PES data from Rb_xC_{70} as an example with which to highlight the similarities and differences between the fullerides formed between C_{60} and the higher fullerenes studied to date.

Figure 14 we show the PES and C 1s excitation spectra of Rb_xC_{70} [47]. On intercalation with Rb, it is clear that charge transfer from the Rb atoms to the fullerene molecules takes place, with the intensity of the first feature in the C 1s excitation spectrum decreasing concurrently with the appearance of a new feature between the HOMO and E_F in the PES spectra. Under these conditions intercalation is complete at $x \sim 6$, with a clear gap separating the now occupied LUMO-derived states from E_F in the PES spectrum. The Rb_xC_{70} samples studied here were produced by sequential evaporation of alkali metal onto a fullerene film, and thus, from our earlier experiences with C_{60} fulleride formation, we would

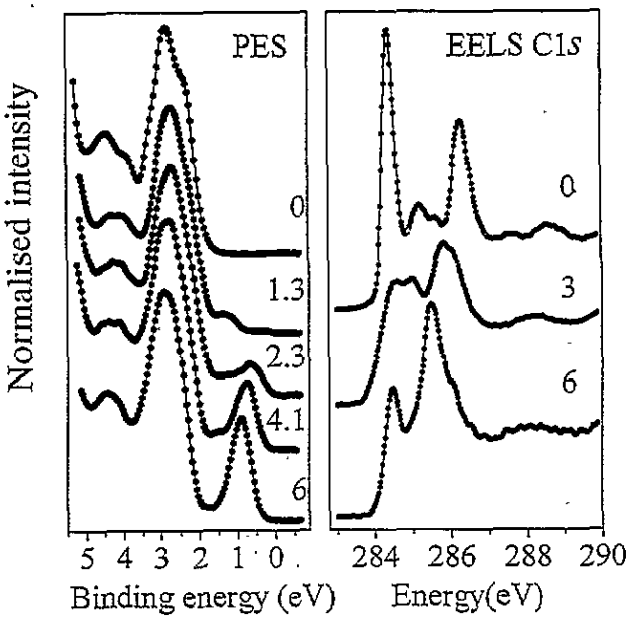

Figure 14. The PES (left-hand panel, $h\nu = 21.22$ eV) and C 1s excitation spectra (right-hand panel) of Rb_xC_{70}, with approximate x values as shown. The data are normalized to the spectral weight of the HOMO-derived feature (PES) and the C 1s $\rightarrow \sigma^*$ edge, located at ~290 eV (EELS), respectively, and offset in the y direction.

expect a degree of phase mixture in these samples. This means that the spectra shown in figure 14 are not necessarily those of the single crystallographic phases represented by the indicated x values. In addition, it is still unknown which are the equilibrium phases in the Rb–C_{70} system.

What is clear from the PES spectra, however, is that in contrast with the case of A_xC_{60} (A = K, Rb, $x \sim 3$), there is at no stage a clear spectral signature of a metallic system—i.e. there is no well defined, sharp cut-off at E_F, in agreement with the lack of a plasmon associated with charge carriers in the valence band excitations of the Rb_xC_{70} system [47]. The same behaviour has also been observed in the K–C_{70} system, in which PES studies of phase pure samples prepared using vacuum distillation showed that at room temperature KC_{70}, K_4C_{70} and K_6C_{70} are stable, with a K_3C_{70} phase stable only at elevated temperature [16]. If the conclusions drawn from the K–C_{70} system also apply here, the broad feature in the electron removal (PES) spectrum at ~1.2 eV seen for $x \sim 1.3$ in figure 14 is characteristic of RbC_{70}, with the peaks at ~0.75 and ~0.9 eV developing on increasing Rb intercalation characterizing the LUMO-derived spectral weight of Rb_4C_{70} and Rb_6C_{70}, respectively. The 'Rb_3C_{70}' C 1s excitation spectrum shown in figure 14 would then represent that of a mixture of the RbC_{70} and Rb_4C_{70} phases. Following the procedure used for C_{60} [34, 37], U has been determined to be ~1 eV for C_{70} [57]—thus also placing this fullerene in the strongly correlated regime and providing a possible cause of the non-metallic nature of the A–C_{70} (A = K, Rb) materials, as has been suggested for A = K [16].

The situation, not least as regards the theoretical treatment of A_xC_{70} electronic structure, is complicated by the lower degeneracy of C_{70}. For example, the first set of A_xC_{70} electron addition states, that are seen to be able to accommodate up to six electrons, cannot be

derived from a single degenerate group of C_{70} molecular orbitals with the same symmetry (unlike the t_{1u}-derived states of C_{60}), as the maximum orbital degeneracy allowed by C_{70}'s D_{5h} molecular symmetry is twofold [125]. The C_{70} 'LUMO'-derived states most probably arise instead from the overlap of three low-lying unoccupied molecular orbitals.

As mentioned at the start of this section, the intercalation compounds of other higher fullerenes besides C_{70} have also been studied using high-energy spectroscopies. In all cases, electron removal spectra consistent with non-metallic behaviour have been observed. The dual advantages of high-energy spectroscopies such as PES, that one can work with very small quantities of higher fullerenes and in an 'atmosphere' (i.e. UHV) in which alkali fullerides are stable, allow the investigation of the intercalation compounds of higher fullerenes long before sufficient quantities are available for detailed bulk measurements. This can mean, however, that although such measurements provide a valuable 'screening' procedure for the discovery of more metallic and possibly superconducting fullerides, a full understanding of the physics of these materials may often require information from complementary sources.

A further field in which an early contribution has been made by high-energy spectroscopy is that of endohedral fullerenes. Here the separation and purification procedures are even more difficult than for the 'empty' higher fullerenes, thus resulting in the worldwide availability even in the case of the most easily prepared materials such as $La@C_{82}$ of only a few milligrams. This material has proved to be stable with respect to thermal evaporation in UHV and so has been studied using PES [126, 127]. Comparison of the spectra of C_{82} and the endohedral show that inclusion of the La ion (XPS studies show that the La atom is electronically very similar to that in La_2O_3 [128]) results in the appearance of new electron removal states between the C_{82} HOMO and E_F—i.e. there is charge transfer from the La atom to the C_{82} cage. These states, however, do not cut the Fermi level, signalling the non-metallic nature of condensed $La@C_{82}$ [126, 127]. In addition, the presence of the La atom also results in modification of the fullerene's electronic states up to as much as 15 eV below E_F, showing that endohedral inclusion is more complex than just an 'electron doping' of the host molecule [127]. Nevertheless, in the context of the electronic structure and properties of A_3C_{60} discussed above, it would still be an interesting thought experiment to include a 3^+ ion such as La inside a fullerene which had threefold LUMO degeneracy—and hence build a solid from $(fullerene)^{3-}$ molecules in which the LUMO-derived band is exactly half full in order to test whether such an idealized, electronically stoichiometric system would be metallic and superconducting, or rather a Mott–Hubbard insulator. The next fullerene with I_h symmetry after C_{60} is C_{120}, so we may need to wait a while before being able to try out such ideas in practice.

The experience of the first attempts at higher fullerene intercalation, together with the more extensively researched A_xC_{60} materials, suggests that the question of why the A_4C_{60}, A_xC_{70}, A_xC_{76}, A_xC_{82} etc materials are non-metallic should be rewritten as 'why out of all the fullerene intercalation compounds without significant guest/host hybridization are alone the A_3C_{60} (A = K, Rb etc) systems metallic *and* superconducting?'

7. *Summary and future directions*

In this review we have tried to relate some of the current issues in the field of the solid state electronic structure of fullerenes and fullerene compounds as probed using high-energy spectroscopies such as PES and EELS. The development of unintercalated fullerene electronic structure in the solid state is shown to follow from that of the molecules themselves, displaying many of the hallmarks of molecular solids including the retention

of molecular-like dipole selection rules for interband transitions and the importance of both exciton formation and electron–vibron coupling. The weak intermolecular overlap is also seen to result in narrow bands, which taken in combination with the relatively large on-site Coulomb correlation energy places solid fullerenes in the highly correlated regime.

We have highlighted the discussion surrounding the role of electron correlation in the determination of the electronic structure of the intercalated fullerenes, with particular reference to the electron removal and addition spectra of A_3C_{60} (A = K, Rb). The possible reasons for the non-metallic nature of A_4C_{60} (A = alkali metal) were also discussed in the light of the clear lifting of the degeneracy of the electronic levels near E_F observed in the EELS spectra of phase pure samples.

The trends towards the increasingly 'graphitic' nature of unintercalated fullerenes as molecular size increases have been discussed with reference to high-energy spectroscopic data from solid C_{60}, C_{70}, C_{76} and C_{84} and the development of the electronic structure of intercalated higher fullerenes has been illustrated with the example of Rb_xC_{70}.

As ever, the investigations outlined above have raised as many questions as they have answered. A few proposals spring to mind as worthy of immediate attention, such as the further investigation of the AC_{60} (A = K, Rb) 'orthopolymer' systems, particularly as a function of temperature; investigation of the electronic structure of C_{60} photopolymer and the study and comparison of isomer-separated higher fullerenes to shed light on the role played by the polyisomeric nature of many of the early samples. In the search for further metallic and possibly superconducting fullerides, the AE–C_{70} (AE = alkaline-earth) systems should be looked at, as well as intercalation compounds of higher fullerenes with high molecular symmetry. In the near future, these and other questions will be occupying us and other groups employing high-energy spectroscopies to study the electronic structure of fullerenes and their compounds in order to try to contribute to the deeper understanding of these fascinating materials.

Acknowledgments

We are very grateful to a number of people for the provision of high-quality fullerene material and its characterization. W Krätschmer (MPI für Astrophysik, Heidelberg) and P Adelmann, G Roth and P Schweiß (Forschungszentrum Karlsruhe) provided C_{60} and C_{60}/C_{70} mixtures for the very first experiments we conducted in 1991, and the latter three also aided in the characterization of the pure C_{70}, C_{76} and C_{84} for which we are indebted to the members of M M Kappes' group in the University of Karlsruhe (in particular R Michel). Thanks to Georg Gensterblum (Namur) for passing on his know-how of film growth in the C_{60}/GeS(001) system. We have received valuable theoretical support in particular from O Gunarsson, together with V Eyert, A I Liechtenstein and V P Antropov (MPI-Stuttgart) and have profited from many discussions with S-L Drechsler (IFW Dresden). Experimental assistance has been gratefully received from R Seeman and R L Johnson (HASYLAB), A Roberts and D Hoad (UMIST), B Scheerer (Forschungszentrum Karlsruhe) and M Surman, D Teehan and M Roper (DRAL, Daresbury Laboratory). Our thanks to all the colleagues who made their results available prior to publication. MSG is grateful for funding under the European Commission's 'Human Capital and Mobility' programme.

References

[1] Kroto H W, Heath J R, O'Brien S C, Curl R F and Smalley R E 1985 *Nature* **318** 162

[2] We also beg the understanding of those whose work has not been cited—the tremendous output in the fullerene field has made exhaustive reviews all but impossible.
[3] Krätschmer W, Lamb L D, Fostiropoulos K and Huffman D R 1990 *Nature* **347** 354
[4] 1992 *J. Phys. Chem. Solids* **53** 1321–485
1992 *Accounts Chem. Res.* **25** 98–175
Both of these contain many excellent overview articles.
[5] Weaver J H and Poirier D M 1994 *Solid State Physics* vol 48, ed H Ehrenreich and F Saepen (New York: Academic) ch 1
[6] See e.g.
Zhou O and Cox D E 1992 *J. Phys. Chem. Solids* **53** 1373 and references therein
[7] See e.g.
Pickett W E 1994 *Solid State Physics* vol 48, ed H Ehrenreich and F Saepen (New York: Academic) p 225 and references therein
[8] Erwin C E 1994 *Buckminsterfullerenes* ed W E Billups and M A Ciufolini (New York: VCH) ch 9 and references therein
[9] Weaver J H 1992 *J. Phys. Chem. Solids.* **53** 1433
[10] Wudl F 1992 *Accounts Chem. Res.* **25** 157
[11] Fink J 1989 *Adv. Electron. Electron Phys.* **75** 121
[12] See e.g.
1978 *Springer Topics in Applied Physics* vol 26, ed M Cardona and L Ley (Berlin: Springer)
Hüfner S 1995 *Springer Series in Solid State Sciences* vol 82 (Berlin: Springer)
[13] Michel R H, Schreiber H, Gierden R, Hennrich R, Rockenberger F, Beck R D, Kappes M M, Lehner C, Adelmann P and Armbruster J F 1994 *Ber. Bunsenges. Phys. Chem.* **98** 975
[14] See e.g.
Diederich F, Ettl R, Rubin Y, Whetten R L, Beck R, Alvarez M, Anz S, Sensharma D, Wudl F, Khemani K C and Koch A 1991 *Science* **252** 548
Kikuchi K, Nakahara Y, Honda M, Suzuki S, Saito K, Shiromaru H, Yamauchi K, Ikemoto I, Kuramochi T, Hino S and Achiba Y 1991 *Chem. Lett.* **16** 1607
Kikuchi K, Nakahara Y, Wakabayashi T, Honda M, Matsumiya H, Moriwaki T, Suzuki S, Shiromaru H, Saito K, Yamanouchi K, Ikemoto I and Achiba Y 1991 *Chem. Phys. Lett.* **188** 177
Taylor R, Langley G J, Avent A G, John T, Dennis S, Kroto H W and Walton D R 1991 *J. Chem. Soc. Perkins Trans.* **2** 1029
[15] Poirier D M 1994 *Appl. Phys. Lett.* **64** 1356
[16] Knupfer M, Poirier D M and Weaver J H 1994 *Phys. Rev.* B **49** 8464
[17] Saito S and Oshiyama A 1991 *Phys. Rev. Lett.* **66** 2637
[18] Troullier N and Martins J L 1992 *Phys. Rev.* B **46** 1754
[19] Fleming R M, Siegrist T, Marsh P M, Hessen B, Kortan A R, Murphy D W, Haddon R C, Tycko R, Dabbagh G, Mujsce A M, Kaplan M L and Zahurac S M 1991 *Mater. Res. Soc. Symp. Proc.* vol 206 (Pittsburgh, PA: Materials Research Society) p 691
Heiney P A, Fischer J A, McGhie A R, Romanow W J, Denenstein A M, McCauley J P, Smith A B and Cox D E 1991 *Phys. Rev. Lett.* **66** 2911
[20] Satpathy S, Antropov V P, Andersen O K, Jepsen O, Gunnarsson O and Lichtenstein A I 1992 *Phys. Rev.* B **46** 1773
[21] Zhu Q, Zhou O, Bykovetz N, Fischer J E, McGhie A R, Romanow W J, Lin C J, Strongin R M, Cichy M A and Smith A B 1993 *Phys. Rev.* B **47** 13984
[22] Chauvet O, Oszlányi G, Forró L, Stephens P W, Tegze M, Faigel G and Jánossy A 1994 *Phys. Rev. Lett.* **72** 2721
[23] For an overview see
Murphy D W, Rosseinsky M J, Fleming R M, Tycko R, Ramirez A P, Haddon R C, Siegrist T, Dabbagh G, Tully J C and Walstedt R E 1992 *J. Phys. Chem. Solids* **53** 1321
[24] Schlüter M, Lannoo M, Needels M, Baraff G A and Tománek D 1992 *J. Phys. Chem. Solids* **53** 1473
[25] Erwin S C and Pickett W E 1991 *Science* **254** 842
[26] Martins J L and Troullier N 1992 *Phys. Rev.* B **46** 1766
[27] Erwin S C and Pederson M R 1991 *Phys. Rev. Lett.* **67** 1610
[28] Benning P J, Stepniak F and Weaver J H 1993 *Phys. Rev.* B **48** 9086
[29] David W I F, Ibberson R M, Matthewman J C, Prassides K, Dennis T J S, Hare J P, Kroto H W, Taylor R and Walton D R M 1991 *Nature* **353** 147
[30] Stephens P W, Mihaly L, Lee P L, Whetten R L, Huang S-M, Kaner R, Diederich F and Holczer K 1991

Nature **351** 632
[31] Gelfand M P and Lu J P 1992 *Phys. Rev. Lett.* **68** 1050
[32] Mele E J and Erwin S C 1994 *Phys. Rev.* B **50** 2150
[33] Shirley E L and Louie S G 1993 *Phys. Rev. Lett.* **71** 133
[34] Lof R W, van Veenendaal M A, Koopmans B, Jonkman H T and Sawatzky G A 1992 *Phys. Rev. Lett.* **68** 3924
[35] Merkel M, Knupfer M, Golden M, Fink J, Seemann R and Johnson R L 1993 *Phys. Rev.* B **47** 11470
[36] Lof R W, Jonkman H T and Sawatzky G A unpublished
[37] Bruhwiler P, Maxwell A J, Mårtensson N and Gunnarsson O 1993 *Phys. Rev.* B **48** 18296
[38] Lu J P 1994 *Phys. Rev.* B **49** 5687
[39] Meinders M B J 1994 *PhD Thesis* University of Grongingen
[40] Brühwiler P A, Maxwell A J, Rudolf P, Gutleben C D, Wästberg B and Mårtensson N 1994 *Phys. Rev. Lett.* **71** 3721
[41] Antropov V P, Gunnarsson O and Jepsen O 1992 *Phys. Rev.* B **46** 13647
[42] van den Brink J, Meinders M B J, Lorenzana J and Sawatzky G A unpublished
[43] Jahn–Teller distortion should also be considered for configurations in which the HOMO level contains one or more holes, such as the final state of a C_{60} electron removal (PES) experiment.
[44] Manini N, Tosatti E and Auerbach A 1994 *Phys. Rev.* B **49** 13008
[45] Gunnarsson O 1995 *Phys. Rev.* B **51** 3493
[46] Gunnarsson O, Handschuh H, Bechthold P S, Kessler B, Ganteför G and Eberhardt W 1995 *Phys. Rev. Lett.* **74** 1875
[47] Sohmen E, Fink J, Baughman R H and Krätschmer W 1992 *Z. Phys.* B **86** 87
Sohmen E, Fink J and Krätschmer W 1992 *Europhys. Lett.* **17** 51
Sohmen E and Fink J 1993 *Phys. Rev.* B **47** 14532
[48] Lichtenberger D L, Jatcko M E, Nebesny K W, Ray C D, Huffman D R and Lamb L D 1991 *Mater. Res. Soc. Symp. Proc.* vol 206 (Pittsburgh, PA: Materials Research Society) p 673
[49] Wertheim G K, Rowe J E, Buchanan G N E, Chaban E E, Hebard A F, Kortan A R, Makhija A V and Haddon R C 1991 *Science* **252** 1419
[50] Chen C-T, Tjeng L H, Rudolf P, Meigs G, Rowe J E, Chen J, McCauley J P, Smith A B, McGhie A R, Romanow W J and Plummer W E 1991 *Nature* **352** 603
[51] Takahashi T, Morikawa T, Sato S, Katayama-Yoshida H, Yuyama A, Seki K, Fujimori H, Hino S, Hasegawa S, Kamiya K, Inokuchi H, Kikuchi K, Suzuki S, Ikemoto K and Achiba Y 1991 *Physica C* **185–189** 417
[52] Weaver J H, Martins J-L, Komeda T, Chen Y, Troullier N, Ohno T R, Kroll G H, Haufler R E and Smalley R E 1991 *Phys. Rev. Lett.* **66** 1741
[53] Terminello L J, Shuh D K, Himpsel F J, Lapiano-Smith D A, Stöhr J, Bethune D S and Meijer G 1991 *Chem. Phys. Lett.* **182** 491
[54] Benning P J, Weaver J H, Chibante L P F and Smalley R E 1991 *Science* **252** 1417
[55] Golden M S, Knupfer M, Fink J, Armbruster J F, Cummins T R, Romberg H A, Roth M, Schmidt M, Sing M, Sohmen E, Michel R, Hennrich F, Rockenberger J, Kappes M M, Hoad D R C, Roberts A J, Roper M, Surman M and Teehan D A 1994 *Mol. Mater.* **4** 51
[56] Armbruster J F, Roth M, Romberg H A, Sing M, Schmidt M, Golden M S, Adelmann P, Schweiss P, Fink J, Michel R, Rockenberger J, Hennrich F and Kappes M M 1994 *Phys. Rev.* B **50** 4933
[57] See e.g.
Knupfer M, Poirier D M and Weaver J H 1994 *Phys. Rev.* B **49** 2281 and references therein
[58] Hino S, Matsumoto K, Hasegawa S, Kamiya K, Inokuchi H, Morikawa T, Takahashi T, Seki K, Kikuchi K, Suzuki S, Ikemoto I and Achiba Y 1992 *Chem. Phys. Lett.* **190** 169
[59] Armbruster J F, Romberg H A, Schweiss P, Adelmann P, Knupfer M, Fink J, Michel R H, Rockenberger J, Hennrich F, Schreiber H and Kappes M 1994 *Z. Phys.* B **95** 469
[60] Jost M B, Troullier N, Poirier D M, Martens J-L, Weaver J H, Chibante L P F and Smalley R E 1991 *Phys. Rev.* B **44** 1966
[61] Zeppenfeld K 1971 *Z. Phys.* **243** 229
[62] Li D, Velasquez S and Schnatterly S E 1994 *Phys. Rev.* B 49 2969
[63] Romberg H A, Sohmen E, Merkel M, Knupfer M, Alexander M, Golden M S, Adelmann P, Pietrus T, Fink J, Seemann R and Johnson R L 1993 *Synth. Met.* **56** 3038
[64] Poirier D M, Weaver J H, Kikuchi K and Achiba Y 1993 *Z. Phys.* D **26** 79
[65] Gensterblum G, Yu L-M, Pireaux J J, Thiry P A, Caudano R, Vigneron J P, Lambin Ph, Lucas A A and Krätschmer W 1991 *Phys. Rev. Lett.* **67** 2171
[66] Skumanich A 1991 *Chem. Phys. Lett.* **182** 486

[67] Hare J P, Kroto H W and Taylor R 1991 *Chem. Phys. Lett.* **177** 394
[68] Takahashi T, Sujuki S, Morikawa T, Katayama-Yoshida H, Hasegawa S, Inokuchi H, Seki K, Kikuchi K, Suzuki S, Ikemoto K and Achiba Y 1992 *Phys. Rev. Lett.* **68** 1232
[69] Bohnen K-P unpublished
[70] Wu J, Shen Z-X, Dessau D S, Cao R, Marshall D S, Pianetta P, Lindau I, Yang X, Terry J, King D M, Wells B O, Elloway D, Wendt H R, Brown C A, Hunziker H and de Vries H S 1992 *Physica* C **197** 251
[71] Themlin J-M, Bouzidi S, Coletti F, Debever J-M, Gensterblum G, Yu L-M, Pireaux J J and Thiry P A 1992 *Phys. Rev.* B **46** 15 602
[72] Gensterblum G, Yu L M, Pireaux J J, Thiry P A, Caudano R, Buslaps T, Johnson R L, Le Lay G, Aristov V, Günther R, Taleb-Ibrahimi A, Indlekofer G and Petroff Y 1993 *Phys. Rev.* B **48** 14 756
[73] Benning P J, Olsen C G, Lynch D W and Weaver J H 1994 *Phys. Rev.* B **50** 11 239
[74] Golden M S, Knupfer M, Fink J, Armbruster J F, Cummins T R, Romberg H A, Roth M, Schmidt M, Sing M, Michel R, Rockenberger J, Hennrich F, Schreiber H and Kappes M M 1994 *Progress in Fullerene Research* ed H Kuzmany, J Fink, M Mehring and S Roth (Singapore: World Scientific) p 309
[75] Lichtenberger D L, Nebesny K W, Ray C D, Huffman D R and Lamb L D 1991 *Chem. Phys. Lett.* **176** 203
[76] The relatively large ionization potential of C_{60} [75] underlies the lack of C_{60} fullerene host/guest complexes in which the carbon cage is positively charged, even when using such aggressive electron acceptors as SbF_5—see e.g.
Datars W R, Chien T R, Nkum R K and Ummat P K 1994 *Phys. Rev.* B **50** 4937
[77] De Seta M and Evangelisti F 1993 *Phys. Rev. Lett.* **71** 2477
[78] Wertheim G K, Buchanan D N E 1993 *Phys. Rev.* B **47** 12 912
[79] Morikawa T and Takahashi T 1993 *Solid State Commun.* **87** 1017
[80] Molodtsov S L, Casado C, Davila M E, Moreno M, Soria M and Ascensio M C 1994 *J. Phys.: Condens. Matter* **6** 925
[81] Takahashi T, Morikawa T, Katayama-Yoshida H, Hasegawa S and Inokuchi H 1992 *J. Phys. Chem. Solids* **53** 1699
[82] Hino S, Matsumoto K, Hasegawa S, Iwasaki K, Yakushi K, Morikawa T, Takahashi T, Seki K, Kikuchi K, Suzuki S, Ikemoto I and Achiba Y 1993 *Phys. Rev.* B **48** 8418
[83] Weaver J H, Benning P J, Stepniak F and Poirier D M 1992 *J. Phys. Chem. Solids* **53** 1707
[84] Poirier D M, Ohno T R, Kroll G H, Chen Y, Benning P J, Weaver J H, Chibante J P F and Smalley R E 1991 *Science* **253** 646
[85] Weaver J H, Poirier D M and Zhao Y B 1993 *Springer Series in Solid State Sciences* vol 117, ed H Kuzmany, J Fink, M Mehring and S Roth (Berlin: Springer) p 146
[86] Poirier D M and Weaver J H 1993 *Phys. Rev.* B **47** 10 959
[87] Tycko R, Dabbagh G, Rosseinsky M J, Murphy D W, Fleming R M, Ramirez A P and Tully J C 1991 *Science* **253** 884
[88] See e.g.
Pichler T, Matus M, Kürti J and Kuzmany H 1992 *Phys. Rev.* B **45** 13 841
[89] See e.g.
Pichler T, Winkler R and Kuzmany H 1994 *Phys. Rev.* B **49** 15 879
[90] Stephens P W, Bortel G, Faigel G, Tezge M, Jánossy A, Pekker S, Oszlányi G and Forró L 1994 *Nature* **370** 636
[91] See e.g.
Pekker S, Jánossy A, Mihaly L, Chauvet O, Carrard M and Forró L 1994 *Science* **265** 1077
[92] Knupfer M, Armbruster J F, Romberg H A and Fink J 1995 *Synth. Met.* **70** 1321
[93] Knupfer M, Fink J, Armbruster J F and Romberg H A 1995 *Z. Phys.* B **98** 9
[94] Knupfer M, Fink J and Armbruster J F 1995 in preparation
[95] Benning P J, Stepniak F, Poirier D M, Martens J L, Weaver J H, Chibante L P F and Smalley R E 1993 *Phys. Rev.* B **47** 13 843
[96] De Seta M and Evangelisti F 1995 *Phys. Rev.* B **51** 1096
[97] Stepniak F, Benning P J, Poirier D M and Weaver J H 1993 *Phys. Rev.* B **48** 1899
[98] Haddon R C, Perel A S, Morris R C, Chang S-H, Fiory A T, Hebard A F, Palstra T T M and Kochanski G P 1994 *Chem. Phys. Lett.* **218** 100
[99] Strictly speaking, the C 1s excitations shown in figure 8 are charge neutral excitations. The IPES spectrum would represent the true electron addition spectrum.
[100] Knupfer M, Merkel M, Golden M S, Fink J, Gunnarsson O and Antropov V P 1993 *Phys. Rev.* B **47** 13 944
[101] A gradual transfer of spectral weight to higher energies, away from the coherent 'single-particle' peak at E_F, has been observed in the electron removal spectra of a series of $3d^1$ transition metal oxides, in

which the effective value of U/W could be increased until the Mott transition is crossed. See
Fujimori A, Hase I, Namatame H, Fujishima Y, Tokura Y, Eisaki H, Uchida S, Takegahara K and de Groot F M F 1992 *Phys. Rev. Lett.* **69** 1796
[102] Cummins T R, Armbruster J F, Golden M S, Knupfer M, Romberg M A, Sing M and Fink J 1994 *Physica* C **235–240** 2491
[103] Kresin V V and Kresin V Z 1994 *Phys. Rev.* B **49** 2715
[104] See e.g.
Sprosser-Prou J and Fink J 1989 *Phys. Rev.* B **40** 10 181
[105] Gunnarsson O, Lichtenstein A I, Eyert V, Knupfer M, Fink J and Armbruster J F 1995 submitted
[106] Kiefl R F, Duty T L, Schneider J W, MacFarlane A, Chow K, Elzey J W, Mendels P, Morris G D, Brewer J H, Ansaldo E J, Niedermayer C, Noakes D R, Stronach C E, Hitti B and Fischer J E 1992 *Phys. Rev. Lett.* **69** 2005
[107] Benning P J, Stepniak F and Weaver J H 1993 *Phys. Rev.* B **48** 9086
[108] For example in our earlier PES work [35] we could not attribute a unique spectral signature to the $x = 4$ phase. Other early PES studies also missed the A_4C_{60} phase for K and Rb [50, 84].
[109] Erwin S C and Bruder C 1994 *Physica* B **199–200** 600
[110] Rudolf P 1995 *PhD Thesis* Facultés Universiatires Notre-Dame de la Paix, Namur
[111] Kortan A R, Kopylov N, Glarum S, Gyorgy E M, Ramirez A P, Fleming R M, Thiel F A and Haddon R C 1992 *Nature* **355** 529
[112] Kortan A R, Kopylov N, Glarum S, Gyorgy E M, Ramirez A P, Fleming R M, Zhou O, Thiel F A, Trevor P L and Haddon R C 1992 *Nature* **360** 566
[113] Chen Y, Poirier D M, Jost M B, Gu C, Ohno T R, Martins J L, Weaver J H, Chibante L P F and Smalley R E 1992 *Phys. Rev.* B **46** 7961
[114] Erwin S C and Pederson M R *Phys. Rev.* B **47** 14 657
[115] Saito S and Oshima A 1993 *Phys. Rev. Lett.* **71** 121
[116] Wertheim G K, Buchanan G N E and Rowe J E 1992 *Science* **258** 1638
[117] Knupfer M, Stepniak F and Weaver J H 1994 *Phys. Rev.* B **49** 7620
[118] Romberg H A, Roth M and Fink J 1994 *Phys. Rev.* B **49** 1427
[119] Jiang L-Q and Koel B E 1994 *Phys. Rev. Lett.* **72** 140
[120] Takahashi T, Morizawa T, Hasegawa S, Kamiya K, Fujimoto H, Hino S, Seki K, Katayama-Yoshida H, Inokuchi H, Kikuchi K, Suzuki S, Ikemoto K and Achiba Y 1992 *Physica* C **190** 205
[121] Benning P J, Poirier D M, Ohno T R, Chen Y, Jost M B, Stepniak F, Kroll G H, Weaver J H, Fure J and Smalley R E 1992 *Phys. Rev.* B **45** 6899
[122] Hino S, Matsumoto K, Hasegawa S, Kamiyawa K, Inokuchi H, Morikawa T, Takahashi T, Seki K, Kikuchi K, Suzuki S, Ikemoto I and Achiba Y 1992 *Chem. Phys. Lett.* **197** 38
[123] Hino S, Matsumoto K, Hasegawa S, Inokuchi H, Morikawa T, Takahashi T, Seki K, Kikuchi K, Suzuki S, Ikemoto I and Achiba Y 1992 *Chem. Phys. Lett.* **190** 169
[124] Hino S, Takahashi H, Iwasaka K, Miyazaki T, Kikuchi K and Achiba Y 1994 *Chem. Phys. Lett.* **230** 165
[125] See e.g.
Saito S and Oshiyama A 1991 *Phys. Rev.* B **44** 11 532
Andreoni W, Gygi F and Parrinello M 1992 *Chem. Phys. Lett.* **189** 241
[126] Hino S, Takahashi H, Iwasaki H, Matsumoto K, Miyazaki T, Hasegawa S, Kikuchi K and Achiba Y 1993 *Phys. Rev. Lett.* **71** 4261
[127] Poirier D M, Knupfer M, Weaver J H, Andreoni W, Laasonen K, Parrinello M, Bethune D S, Kikuchi K and Achiba Y 1994 *Phys. Rev.* B **49** 17 403
[128] Weaver J H, Chai Y, Krol G H, Jin C, Ohno T R, Haufler R E, Guo T, Alford J M, Conceicao J, Chibante L P F, Jain A, Palmer G and Smalley R E 1992 *Chem. Phys. Lett.* **190** 460
Guo T, Diener M D, Chai Y, Alford M J, Haufler R E, McClure S M, Ohno T R, Weaver J H, Scuseria G E and Smalley R E 1992 *Science* **257** 1661